The Arabidopsis mTERF-repeat MDA1 protein plays a dual function in transcription and stabilization of specific chloroplast transcripts within the and operons

Louis-Valentin Meteignier, Rabea Ghandour, Karin Meierhoff, Aude Zimmermann, Johana Chicher, Nicolas Baumberger, Abd El Malek Alioua, Jörg Meurer, Reimo Zoschke, Kamel Hammani

DR KAMEL HAMMANI (Orcid ID : 0000-0001-5759-5955)

Article type : Regular Manuscript

The Arabidopsis mTERF-repeat MDA1 protein plays a dual function in transcription and stabilization of specific chloroplast transcripts within the *psbE* and *ndhH* operons

Louis-Valentin Méteignier[1], Rabea Ghandour[2], Karin Meierhoff[3], Aude Zimmerman[1], Johana Chicher[4], Nicolas Baumberger[1], Abdelmalek Alioua[1], Jörg Meurer[5], Reimo Zoschke[2], Kamel Hammani[1]

[1]Institut de Biologie Moléculaire des Plantes, Centre National de la Recherche Scientifique (CNRS), Université de Strasbourg, 12 rue du Général Zimmer, 67084 Strasbourg, France

[2]Max Planck Institute of Molecular Plant Physiology, Am Mühlenberg 1, 14476 Potsdam-Golm, Germany

[3]Institute of Developmental and Molecular Biology of Plants, Heinrich Heine University Düsseldorf, 40225 Düsseldorf, Germany

[4]Plateforme protéomique Strasbourg Esplanade FRC1589 du CNRS, Université de Strasbourg, 15 rue René Descartes, 67084 Strasbourg, France

[5]Plant Sciences, Faculty of Biology, Ludwig-Maximilians-University Munich, Großhaderner Street 2-4, 82152 Planegg-Martinsried, Germany

Author for correspondence: Kamel Hammani Tel: +333 67 15 52 81 Email: kamel.hammani@ibmp-cnrs.unistra.fr

Received: *31 March 2020*

Accepted: *15 April 2020*

ORCID ID:

Louis-Valentin Méteignier: 0000-0001-9639-5737
Karin Meierhoff : 0000-0001-5273-7651
Johana Chicher: 0000-0002-4403-7484
Nicolas Baumberger: 0000-0003-3459-4532
Jörg Meurer: 0000-0003-2973-9514
Reimo Zoschke: 0000-0002-6898-6836
Kamel Hammani: 0000-0001-5759-5955

Summary

- The mTERF gene family encodes for nucleic acid binding proteins that are predicted to regulate organellar gene expression in eukaryotes. Despite the implication of this gene family in plant development and response to abiotic stresses, a precise molecular function was assigned to only a handful number of its ~30 members in plants.
- Using a reverse genetics approach in *Arabidopsis thaliana* and combining molecular and biochemical techniques, we revealed new functions for the chloroplast mTERF protein, MDA1.
- We demonstrated that MDA1 associates *in vivo* with components of the plastid-encoded RNA polymerase and transcriptional active chromosome complexes. MDA1 protein binds *in vivo* and *in vitro* with specificity to 27-bp DNA sequences near the 5'-end of *psbE* and *ndhA* chloroplast genes to stimulate their transcription and additionally promote the stabilization of the 5'-ends of processed *psbE* and *ndhA* mRNAs. Finally, we provided evidence that MDA1 function in gene transcription likely coordinates RNA folding and the action of chloroplast RNA binding proteins on mRNA stabilization.
- Our results provide examples for the unexpected implication of DNA binding proteins and gene transcription in the regulation of mRNA stability in chloroplasts blurring the boundaries between DNA and RNA metabolism in this organelle.

Key words

Plastid, mTERF, gene expression, DNA, RNA, helical repeat protein

Introduction

Owing to their endosymbiotic evolution, chloroplasts retained only ~100 genes of their cyanobacterial ancestor genome (Sato *et al.*, 1999) that encode mRNAs of proteins involved in photosynthesis and a small fraction of the components of the chloroplast gene expression machinery (ribosomal proteins, rRNAs, tRNAs, plastid-encoded RNA polymerase). Thus, the expression of chloroplast genes requires the import of hundreds proteins that are encoded by nuclear genes (reviewed in Barkan, 2011). Consistently with their function in gene expression, many of these proteins bind to DNA or RNA *in vivo*. Some of these protein families are only found in eukaryotes and specialized in the regulation of organellar genes (reviewed in Hammani *et al.*, 2014). One such example is the mTERF (mitochondrial transcription termination factor) family. mTERF proteins are made of tandem repeats of a degenerate ~31 amino acids motif that

folds into three helices. These repeats stack to form a superhelix structure that is predicted to accommodate double stranded DNA in its central groove (Jimenez-Menendez *et al.*, 2010; Yakubovskaya *et al.*, 2010). The mTERF family in metazoans includes 4-5 members that have preponderantly been implicated in DNA-related functions in mitochondria like gene transcription or replication (reviewed in Roberti *et al.*, 2009). By contrast, the family expanded to ~30 members in higher plants (Babiychuk *et al.*, 2011; Kleine, 2012; Zhao *et al.*, 2014) and recent studies have suggested that this expansion has been accompanied by a functional diversification in RNA metabolism such as intron splicing and rRNA maturation in organelles (Hammani & Barkan, 2014; Hsu *et al.*, 2014; Romani *et al.*, 2015; Zhang *et al.*, 2018). In addition to these studies, transcriptomic and physiological analyses conducted in Arabidopsis and crop species have highlighted the importance of *mTERF* genes for plant response to a variety of abiotic stresses (Zhao *et al.*, 2014; Zhou *et al.*, 2016; Xu *et al.*, 2017; Robles *et al.*, 2018; Nunez-Delegido *et al.*, 2019). Nevertheless, only a handful of *mTERF* genes have been molecularly and biochemically characterized in plants to comprehensively apprehend their functional diversification. To get deeper understanding of *mTERF* functions in plants, we conducted a reverse genetics approach with genes that had not been clearly characterized. Here, we describe new molecular and biochemical functions for the Arabidopsis mTERF protein, At4g14605, previously known as MDA1 (Robles *et al.*, 2012) or mTERF5 which had been proposed to act as a positive regulator of *psbE-F-L-J* genes transcription in Arabidopsis chloroplasts (Ding *et al.*, 2019). We report the discovery of an additional site of action for MDA1 in *ndhA* gene and evidence for a functional model in which MDA1 promotes the stabilization of the 5'-ends of processed *psbE* and *ndhA* mRNAs besides their gene transcription. These findings provide examples for the unexpected implication of DNA binding proteins and gene transcription in the regulation of mRNA stability in chloroplasts.

Material and Methods

Oligonucleotides used in this study are listed in Table S1.

Plant material

Arabidopsis thaliana ecotype Columbia (Col-0) and *Nicotania benthamiana* were used in this study. The T-DNA insertion mutant allele *mda1-2* (SAIL_425_E03) was obtained from the ABRC Stock Center. The *hcf111-1* allele was retrieved from a collection of EMS mutagenized

Arabidopsis plants displaying high-chlorophyll fluorescence (Meurer *et al.*, 1996). Complemented mutants were obtained via *Agrobacterium tumefaciens* transformation of *mda1-2* homozygote plants. The binary vector (pGWB17) used for Agrobacterium-transformation expressed the At4g14605 coding sequence fused with a 4xMyc C-terminal tag under the control of the CaMV 35S promoter. Transgenic plants were selected on Murashige and Skoog (MS) plates containing 25 μg/ml hygromycin. All experiments were performed using 7-day-old plants grown *in vitro* (1× MS pH 5.7, 0.5% sucrose, 0.8% Agar; 16 h light : 8 h dark cycles; 65-85 μmol photons m^{-2} s^{-1}) or 14 day-old plants grown on soil for immunoprecipitation combined with mass spectrometry experiments. The methods for the plant chlorophyll fluorescence measurements are provided in Methods S1.

Protein extraction and immunoblotting

Total proteins were extracted in Tris pH 7.5, 10% glycerol, 1% NP40, 5 mM EDTA, 2 mM EGTA, 35 mM β-mercaptoethanol, 1× EDTA-free protease inhibitor cocktail (Roche), resolved on SDS-PAGE, and transferred onto PVDF membrane at 80 V for 1.5 h using wet transfer. Anti-PsaD, -PetD antibodies were kindly donated by Alice Barkan (University of Oregon). Anti-NdhL and -NdhB antibodies were kind donations of Toshiharu Shikanai (University of Kyoto) and anti-RbcL antibodies were donated by Géraldine Bonnard (CNRS). Other antibodies against chloroplast proteins were purchased from Agrisera or PhytoAB and anti-Myc antibodies (clone 9E10) from Sigma-Aldrich.

Subcellular localization of MDA1

Nicotiana benthamiana leaves were infiltrated with *Agrobacterium tumefaciens* GV3101 carrying pMDC83*:MDA1* or pB7RWG2*:RAP* at an OD_{600} of 0.5 each. Protoplasts were prepared as in (Berglund *et al.*, 2009) and examined under a Zeiss LSM 780 confocal microscope. GFP was excited at 488 nm and emission was acquired between 493-556 nm. RFP and chlorophyll were excited at 561 nm and emissions were acquired between 588-641 nm and 671-754 nm, respectively.

RNA extraction and analyses

Tissues were ground in liquid nitrogen and RNA was extracted with Trizol following manufacturer's protocol (Invitrogen™). RNA was further extracted with phenol-chloroform pH

4.3. Five μg of Turbo DNase (Thermo Fisher) treated RNAs were used for Superscript IV reverse transcription with random hexamers. The resulting cDNA was diluted 20-fold for qPCR reaction. *ACT2 (AT3G18780)* and *TIP41 (AT1G13440)* were used as reference genes. For RNA gel blotting, five μg (*psbE* operon genes) or 15 μg (*ndhH* operon genes) of RNA was fractionated on 1.2% agarose-1% formaldehyde gel and blotted as described previously (Barkan, 1998). Strand specific 60-mer synthetic DNA oligonucleotides were used as probes (Table S1). For sRNA blotting, five to 10 μg of low-molecular weight RNAs enriched from total leaf RNA as in (Lu *et al.*, 2007) were blotted as described in (Zhelyazkova *et al.*, 2012). Results were visualized on an Amersham Typhoon imager and data quantification was performed with ImageQuant TL (GE Healthcare). Details about the tiling microarray plastid transcriptome and translatome analyses are provided in Methods S1.

RNA structure prediction

Secondary structures were predicted with the mfold server (RNA folding form version 2.3 energies) at http://unafold.rna.albany.edu/ using default parameters and a folding temperature of 25°C.

Chloroplast isolation

Chloroplasts were purified by density gradient and differential centrifugations as described in (Kunst, 1998).

Chloroplast fractionation

Chloroplasts were lysed in 30 mM HEPES-KOH pH 8, 10 mM MgOAc, 60 mM KOAc, 1 mM DTT, 1× EDTA-free protease inhibitor cocktail, 1 mM PMSF with or without the addition of 0.2 M Na_2CO_3, 1% NP-40, 100 μg ml^{-1} RNase A, 250 U ml^{-1} RNase T1 or 50 U ml^{-1} DNase I (Thermo Fisher). Stromal and thylakoid proteins were separated by centrifugation at 20,000 g for 10 min at 4°C.

Transcription run-on assay

The rate of transcription from 5×10^7 chloroplasts was analyzed as in (Zubo *et al.*, 2011). Results were visualized and signals quantified as described before.

CoIP-MS

Chloroplasts were crosslinked in 300 mM Sorbitol, 30 mM HEPES-KOH pH 8, 2 mM DSP for 1 h on ice. Chloroplasts were then resuspended in 20 mM Tris pH 7.5, 150 mM NaCl, 1 mM EDTA, 1% NP-40, 1× EDTA-free protease inhibitor cocktail, 1 mM PMSF, centrifuged 20 min at 21,000 g, 4°C. 2.5 mg of proteins from the supernatant were immunoprecipitated by the addition of 50 µL anti-MYC Miltenyi magnetic beads and incubation for 30 min at 4°C on a rotator. Beads were washed and eluted as recommended by the manufacturer. Eluted proteins were digested with sequencing-grade trypsin (Promega) and analyzed by nanoLC-MS/MS at the "Plateforme Proteomic Strasbourg-Esplanade". Data were processed as described (Lange *et al.*, 2019). A home-made R package IPinquiry was used to identify significant MDA1 protein interactors by a statistical analysis on spectral counts using a negative binomial GLM model as described (Lange *et al.*, 2019). The full list of protein interactants is provided in Table S4.

DIP-qPCR

Chloroplasts were crosslinked in 1 ml of 300 mM Sorbitol, 30 mM HEPES-KOH pH 8, 1% formaldehyde during 30 min on ice. Crosslinking was stopped by adding glycine to 125 mM and incubation on ice for 5 min. Chloroplasts were recovered by centrifugation and lysed in 1ml of DIP buffer (50 mM Tris pH 7.5, 150 mM NaCl, 1 mM EDTA, 1% Triton X100, 0.1% SDS, 0.1% Na-Deoxycholate, 1× EDTA-free protease inhibitor cocktail). Chloroplast DNA was sheared to 0.2-0.8 kb using a bioruptor on high settings, 30 s ON, 30 s OFF, 5 min, four times. 2.5 mg of proteins were used per IP with 50 µL of anti-MYC Miltenyi magnetic beads and incubated on a rotator for 30 min at 4°C. Beads were washed four times with DIP buffer and eluted in 200 µL of hot 100 mM $NaHCO_3$, 1% SDS. Samples were reverse cross-linked by adding 15 µL of 3 M NaCl, overnight incubation at 65°C and subsequent digestion with 20 µg proteinase K, 10 mM EDTA at 37°C for 1 h. RNA was removed by adding 1 µL of RNase A/T1 (Thermo Fisher) and incubation for 15 min at 37°C. DNA from the IP and supernatant fractions was extracted with phenol/chloroform and used at 1:50 dilution in qPCR reactions. Percent recovery was calculated using the formula: $100*2^{-(Ct(IP)-Ct(sup))}$ (Saleh *et al.*, 2008).

Recombinant MDA1 production

MDA1 coding sequence without the first 387 bp that are predicted to encode the chloroplast transit peptide was amplified by PCR on cDNA and cloned into BamHI and SalI in pMAL vector. The recombinant N-terminal MBP fusion protein was expressed in *E. coli* BL21 and purified as described in (Williams-Carrier *et al.*, 2008) except that the lysis buffer contained 250 mM NaCl and did not include CHAPS detergent.

***In vitro* binding assays**

Synthetic DNA or RNA probes (Integrated DNA Technologies) were 5′ end-labeled with [γ-32P]-ATP and T4 polynucleotide kinase and then purified by illustra™ Microspin G-25 column filtration (GE Healthcare). dsDNA or RNA probes <60 bp were obtained by annealing two complementary oligonucleotide sequences. DNA probes >60 bp were amplified by PCR using gDNA as template, agarose gel purified and [γ-32P]-ATP 5'-end labelled as described above. Except where otherwise indicated, rMDA-binding reactions contained 50 mM Tris·HCl pH 7.5, 150 mM KCl, 4 mM DTT, 0.04 mg ml^{-1} BSA, 0.25 mM EDTA, 0.05 mg ml^{-1} poly(dI-dC) competitor, 0.25% Tween-20, 10% (vol/vol) glycerol and 15 pM radiolabeled probe. Poly(dI-dC) was substituted by 10 units of RNasin (Promega) in RNA binding assays. Reactions were incubated for 30 min at 25°C and resolved on 5% native polyacrylamide gels in 1× TBE. DNase I footprint assays were performed in similar binding conditions in 20 μL volumes. First, binding reactions containing 5FAM-end labelled *psbE2* DNA probe in the presence or absence of rMDA (0.5 μM) were incubated for 30 min at 25°C. 10 μL of 0.015 U of DNase I in 0.5 mM $CaCl_2$, 12.5 mM $MgCl_2$ buffer was subsequently added and the reactions incubated for 5 min at 25°C. The reactions were brought to 25 mM EDTA, 0.125% SDS, 200 mM sodium acetate to stop cleavage and DNA fragments were purified by phenol/chloroform extraction and ethanol precipitation. 200 ng of DNA products for each reaction were mixed with 0.33 μL of GeneScan™ 400HD ROX™ dye Size Standard and fractionated by automated fluorescent capillary electrophoresis on an ABI PRISM 3130 XL Genetic Analyzer. Product peaks were aligned with GeneMapper software to a sequencing ladder generated with a USB Thermo Sequenase Cycle Sequencing Kit.

Results

***MDA1* encodes an mTERF-repeat protein required for chloroplast biogenesis**

At4g14605 encodes the chloroplast mTERF protein MDA1 that has been previously implicated in chloroplast development and abiotic stress responses in Arabidopsis but whose molecular function

had not been characterized (Robles *et al.*, 2012). The *MDA1* gene contains four exons and encodes a 493 amino acid protein harboring eight mTERF tandem repeats and a predicted 43 amino acid chloroplast N-terminal transit peptide (Fig. 1a). Homozygote *mda1* mutant plants for the T-DNA insertion line SAIL_425_E03 (*mda1-2*) were obtained. The analysis of the T-DNA flanking sequence tags in *mda1-2* revealed the presence of an inverted T-DNA repeat arrangement inserted in the fourth exon of *MDA1* gene between genomic positions +1133 and +1154. Disruption of *MDA1* led to pale leaf pigmentation and a dwarf phenotype (Fig. 1b). Despite their severe phenotype, the *mda1-2* plants were fertile and produced siliques containing seeds. The introduction of a wild-type copy of *MDA1* gene into *mda1-2* fully restored the wild-type phenotype demonstrating that *mda1-2* phenotype resulted from *MDA1* disruption. RT-PCR experiments conducted on cDNAs from wild-type, *mda1-2* and complemented plants using primers amplifying the full-length *MDA1* gene confirmed that the *mda1-2* mutant is a knockout (Fig. 1c).

A second mutant allele for *MDA1* was independently retrieved from a collection of EMS mutagenized Arabidopsis plants displaying high chlorophyll fluorescence (Meurer *et al.*, 1996) and was designated *hcf111-1*. *hcf111-1* harbors a cytosine to thymine transition in the fourth exon of At4g15605 converting a proline to leucine residue in the last mTERF domain of MDA1 (Fig. 1a). *hcf111-1* plants grown on soil displayed a pale leaf and dwarf phenotype similar to *mda1-2* allele (Fig. S1a).

To establish the intracellular localization of MDA1, an MDA1-GFP fusion protein was transiently expressed in tobacco leaves and leaf protoplasts were examined by confocal microscopy (Fig. 1d). The GFP fusion protein was detected in discrete foci within chloroplasts, which colocalize with the fluorescence signal of a coexpressed chloroplast nucleoid-associated protein RAP, fused with RFP (Kleinknecht *et al.*, 2014). Thus, these results demonstrate that MDA1 localizes to chloroplasts where it is associated with the nucleoids. Immunodetection on chloroplast sub-fractions isolated from complemented mutant plants expressing a 4xMyc epitope tagged version of MDA1 revealed that MDA1 was only detected in the membrane fraction consistent with the association of chloroplast nucleoids to membranes (Fig. S2) (Sato *et al.*, 2003). Altogether, these results indicate that MDA1 is a chloroplast protein and plays an important role in chloroplast biogenesis and plant development.

The accumulation of PSII and NDH subunits is impaired in *mda1* mutants

To identify the defect in chloroplast biogenesis in *mda1* more precisely, we performed immunoblot analyses on individual subunits of chloroplast protein complexes (Photosystem (PS) I and II, NADH dehydrogenase (NDH), Cytochrome b_6f, ATP synthase, Rubisco and the ribosome) (Fig. 2). The immunoblot results showed that subunits of the PSII and NDH complexes were particularly decreased in *mda1-2* (~10% of wild-type level) and that their accumulation is fully restored in the complemented line. In addition, a moderate loss of the PSI subunit PsaD could be observed in *mda1-2*.

To confirm these results, the photosynthetic capacities of the two mutant alleles were measured by fluorometry along with the wild-type and complemented plants. Chlorophyll *a* fluorescence analyses demonstrated that the maximum quantum yield of PSII, expressed as Fv/Fm, was reduced below 0.5 in the mutants indicative of primary defects in PSII (Meurer *et al.*, 1996) (Table S2). This can partially be explained by a three-fold increased Fo level (Table S1). As observed in *psbL*, *psbN* and several other PSII mutants (Meurer *et al.*, 1996; Swiatek *et al.*, 2003; Torabi *et al.*, 2014) the fluorescence dropped to 50% below the initial Fo level and then partially increased during induction again indicating primary defects in PSII. This caused a reduction of the PSII quantum yield (Φ_{PSII}) below 50% of the wild-type and an increase in non-photochemical quenching (NPQ). In order to estimate the rate-limiting step in photosynthetic electron transport, PSI yield (Φ_{PSI}), as well as donor and acceptor side limitation of PSI ([$\Phi_{PSI\ ND}$] and [$\Phi_{PSI\ NA}$], respectively) were measured (Table S2). Whereas Φ_{PSI} was not severely changed, $\Phi_{PSI\ ND}$ was twice as high and $\Phi_{PSI\ NA}$ decreased several-fold in the mutant as compared to the wild-type. This demonstrates that the electron flow towards PSI is rate limiting as it can be expected by the reduced PSII activity. Overall, less than 50% active P700 could be detected in *mda1* mutants as compared to the wild-type. This indicates a partial loss of PSI in the mutants. Both, *mda1-2 and hcf111-1*, behaved almost identically and complemented lines showed the wild-type phenotype indicating complete recovery.

Expression of chloroplast *psbE* and *ndhH* operons is impaired in the *mda1* mutant

mTERF proteins are gene expression regulators in organelles (Kleine & Leister, 2015). To assess whether the loss of PSII and NDH proteins were caused by a defect in chloroplast gene expression, we assessed the accumulation of chloroplast gene transcripts by qRT-PCR in *mda1-2* wild-type and complemented plants (Fig. 3). The results showed that the steady state levels of

specific transcripts from PSII: *psbE*, *psbF*, *psbL*, *psbJ* and NDH genes: *ndhA*, *ndhI* were particularly diminished in *mda1-2* compared to wild-type. The effect of the loss of *MDA1* function on the expression of genes was fully mitigated in the complemented plants. These results correlated well with the specific loss of the PSII and NDH complex in *mda1-2* (Fig. 2). In addition, a chloroplast transcriptome wide-analysis was independently conducted on the *hcf111-1* allele. This analysis measured the RNA steady state level of chloroplast genes in *hcf111-1* compared to wild-type with their translation efficiency by tiling microarrays of the plastid ORFeome (Zoschke *et al.*, 2013) (Fig. S1b and Table S3). The abundance of *psbE*, *psbF*, *psbL*, *psbJ* and *ndhA*, *ndhI* transcripts was specifically affected in *hcf111-1* with a magnitude similar to what was observed for the *mda1-2* allele but their translation was not impacted. Thus, we concluded that mutations in *MDA1* gene compromise the expression of *psbE*, *psbF*, *psbL*, *psbJ, ndhA* and *ndhI* genes.

Most chloroplast genes are organized in operon-like structure and are cotranscribed as polycistronic mRNA precursors whose posttranscriptional maturation gives rise to a variety of overlapping mRNA isoforms (Barkan, 2011). The posttranscriptional processing of these RNA precursors into mature mRNAs rely predominantly upon the cooperative actions of exoribonucleases and RNA binding proteins from the PPR family that block their RNA degradation activity *in vivo* to stabilize the 5' or 3' ends of these processed mRNAs. The RNA fragments bound by these proteins usually accumulate as small RNA footprints (sRNAs) of ~20-30 nt whose 5' or 3' ends coincide with those of the processed mRNAs these proteins stabilize *in vivo* (Ruwe & Schmitz-Linneweber, 2012; Zhelyazkova *et al.*, 2012; Ruwe *et al.*, 2016).

Genes whose expression is affected in *mda1* mutants are located in two independent transcriptional units (Fig. 4). To validate our findings and pinpoint which of the RNA isoforms from these gene clusters were missing in the *mda1* mutant, RNA gel blot hybridization was performed (Fig. 4b, e). RNA blotting with probes for *psbE*, *psbF*, *psbL* and *psbJ* genes revealed a severe reduction of one prominent transcript of 1.1 kb in *mda1-2* which accumulated to WT level in CP plants, while the abundance of an additional 1.4 kb transcript was less affected in the mutant (Fig. 4b and S3). The identical RNA hybridization patterns for the 4 genes indicates that the two transcripts correspond to tetracistronic *psbE-F-L-J* mRNAs, consistent with previous observations (Westhoff *et al.*, 1985; Xiong *et al.*, 2019). The mapping of the transcript ends by circular RT-PCR analysis (Fig. 4c and S4) showed that the defective 1.1 kb transcript is expected to be a 5'-end processed *psbE-F-L-J* mRNA whose 5'-end maps 2 nt downstream of the PEP transcription

initiation site (TSS); located at position -127 from *psbE* ATG (Allorent *et al.*, 2013), and whose 3'-end maps 95 nt downstream the *psbJ* stop codon. In agreement with the RNA blots, the frequency of the 1.1 kb *psbE* mRNA termini was particularly diminished in *mda1* compared to the wild-type but the reduction was more severe for the 5'- than the 3'-end indicating that MDA1 acts primarily on the 5'-end stability of the mature *psbE-F-L-J* mRNA. Additional RNA blotting was conducted to map the 1.4 kb mRNA. Probes hybridizing to the 1.1 kb mRNA UTRs or immediately upstream the 5'-UTR detected the 1.4 kb RNA form whereas a probe hybridizing downstream the *psbJ* 3'-UTR did not reveal any band. The RNA cross-comparison of these hybridizations indicates that most 1.4 kb mRNAs differ from the 1.1 kb mRNAs by a longer 5'-UTR. cRT-PCR using a reverse primer located upstream the -125 *psbE* 5'-end confirmed this and placed a scattered *psbE* 5'-end in the -479 to -152 region, which suggested the existence of an alternative distal TSS (Fig. 4a/c).

Similar experiments were conducted to characterize *ndhA* and *ndhI* RNA accumulation in *mda1* mutant. These genes belong to the *ndhH* gene cluster (Fig. 4d) that gives rise to overlapping RNAs whose positions have been partially mapped (Maria del Campo *et al.*, 2006). The RNA blotting revealed that the abundance of distinct mRNAs containing *ndhA* and *ndhI* was specifically reduced in *mda1* whereas mRNAs containing genes upstream or downstream were barely affected. We were able to assign positions for these disturbed transcripts based on their size, the probes to which they hybridized and the positions of chloroplast RNA termini in Arabidopsis that were mapped in this work or in a recent study (Castandet *et al.*, 2019). Transcripts whose abundance is diminished in *mda1* start with an *ndhA* 5'-end. cRT-PCR mapping of *ndhA* mRNA termini revealed that the frequency of the prominent *ndhA* 5'-end that maps at position -67 in the wild-type is reduced in *mda1* and increased in complemented plants overexpressing MDA1 compared to wild-type (Fig. 4f and S4). The *ndhA* RNA 3'-end mapping at position +58 was reduced as well in *mda1* but to a much lesser extent than the 5'-end. These results argue that MDA1 contributes to the stabilization of the -67 *ndhA* 5'-end *in vivo*. Interestingly, the position of this processed 5'-end coincides with the existence of a recently identified TSS suggesting that the 5'-end processing of *ndhA* mRNA is concomitant to transcription (Castandet *et al.*, 2019).

Additional evidence that MDA1 promotes the posttranscriptional stabilization of the 5' ends of the processed *psbE* and *ndhA* mRNAs comes from the observation that chloroplast sRNAs sharing hallmarks of PPR footprints match the 5'- or 3'-end of the mRNAs that require MDA1 for their accumulation *in vivo* (Ruwe & Schmitz-Linneweber, 2012; Zhelyazkova *et al.*, 2012; Ruwe

et al., 2016) (Fig. 4a, 4d and S4). RNA gel blots were performed to analyze the accumulation of these sRNAs in *mda1* (Fig. 5). *mda1* specifically lacked the sRNAs from the *psbE* and *ndhA* 5'-ends but not from their 3' ends as compared to wild-type and complemented plants. Moreover, sRNAs mapping in other genomic locations (*psaC* and *rbcL*) accumulated normally in the mutant. The specific loss in *mda1* of these two sRNAs that coincide with the 5'-end of processed *psbE* and *ndhA* mRNAs demonstrates that posttranscriptional RNA processing at these sites depends on the presence of MDA1. mTERF proteins are helical-repeat proteins and share structural analogy to PPRs and members of their family have been involved in RNA-related functions in organelles (Hammani & Barkan, 2014; Hsu *et al.*, 2014; Romani *et al.*, 2015; Zhang *et al.*, 2018). Thus, these sRNAs could be MDA1's footprints or MDA1 might promote the *in vivo* binding of PPR proteins to the 5' ends of processed *psbE* and *ndhA* mRNAs.

Altogether, the RNA blotting and end mapping results confirmed that MDA1 supports the *in vivo* accumulation of transcripts containing processed *psbE* and *ndhA* 5'-ends. Nonetheless, the alteration of gene transcription could account for the decrease of the steady-state level of these mRNAs in *mda1*. To determine whether transcriptional changes of these genes applied to *mda1*, chloroplast run-on transcription assays were performed (Zubo *et al.*, 2011). Genes whose transcripts accumulation was defective in *mda1* were selected as probes for hybridization with neosynthesized RNAs along with unaffected genes (Fig. 6a). Run-on results and their quantification showed that the transcription rate of *psbE* and *ndhA* in *mda1* was ~44% and 68% of the wild-type, respectively, whereas transcription of *ndhH* or *psaC* was not affected compared to wild-type and complemented plants. To understand the contribution of this altered transcription to the severe reduction of the processed *psbE-F-L-J* and *ndhA* mRNAs in *mda1*, their relative transcription rates were compared to the transcripts abundance measured by qRT-PCR or RNA gel blots (Fig. 6b). RNA gel blots revealed that the loss of the 1.1 kb *psbE-F-L-J* mRNA in *mda1* was more severe than expected from qRT-PCR analysis. This could be explained by qRT-PCR not being strand specific and by its limitation to distinguish overlapping mRNAs. While the transcription activity of *psbE* and *ndhA* genes in *mda1* were respectively ~44% and 68% of the wild-type, the mutant only accumulates ~3.6% and 24% of their respective mRNAs. Therefore, the decrease of *ndhA* and *psbE* transcription in *mda1* cannot in itself explain the more severe loss of the processed *psbE* and *ndhA* mRNAs *in vivo*. Altogether, the results indicate that MDA1 plays a role in promoting *psbE* and *ndhA* gene transcription as well as contributing to the posttranscriptional stabilization of their 5'-end processed mRNAs *in vivo*.

MDA1 is found in high-molecular weight complexes and associates with TAC components *in vivo*

MDA1 is associated to chloroplast membranes (Fig. S2). To understand the basis for this association, chloroplast membranes were isolated from the complemented plants expressing a 4xMyc tagged version of MDA1 and different treatments were applied to them. The release of MDA1 or the integral thylakoid membrane protein control, PsaD (Sane *et al.*, 2005) to the soluble fraction was monitored by immunoblotting (Fig. 7a). Treatment with RNase or DNase had no effect on the membrane association of MDA1 indicating that MDA1 is not attached to the membranes via its association with DNA or RNA. On contrary, treatments by sodium carbonate or the membrane solubilization agent NP40 detached the protein from the membranes indicating that MDA1 is a peripheral protein as sodium carbonate treatment releases peripheral membrane proteins attached by hydrophobic interactions but not integral membrane proteins (Fujiki *et al.*, 1982).

In order to analyze the association of MDA1 with high-molecular weight complexes in chloroplasts, solubilized chloroplasts were fractionated by sedimentation on sucrose gradients (Fig. 7b). MDA1 was mainly detected in macromolecular complexes ≤0,55 MDa (fractions 3 to 8) and to a lesser extent in complexes of ~1 MDa (fractions 11 to P). DNase and RNase treatments of chloroplast extracts prior to sucrose gradient fractionation reduced the presence of MDA1 in fractions above 6 suggesting that some MDA1 proteins are found in large complexes containing chloroplast DNA and RNA.

To understand the protein composition of MDA1 complexes, coimmunoprecipitation (coIP) was performed on solubilized chloroplasts and proteins from immunoprecipitated fractions were identified by LC-MS/MS (Fig. 7c). Out of 35 proteins that were significantly enriched in MDA1 IPs, 21 were components of the plastid transcriptional active chromosome (TAC) (Pfalz *et al.*, 2006) including the 4 subunits of the plastid encoded RNA polymerase, PEP (RpoA, B, C1 and C2). Immunoblot analysis of anti-Myc coimmunoprecipitates confirmed that RpoB associates with MDA1 in chloroplast extract of the complemented plants (Fig. 7c). MDA1's protein partners supports a function in chloroplast transcription. Altogether, these results in conjunction with *mda1* transcriptomic analyses indicate that MDA1 associates *in vivo* with the TAC complex to promote transcription of specific genes.

MDA1 is a DNA binding protein that associates with *psbE* and *ndhA* genes *in vivo*

Consistent with their function in the regulation of organellar gene expression, several mTERF proteins have been described to bind DNA or RNA (reviewed in Kleine & Leister, 2015). To determine whether MDA1 binds to nucleic acids *in vitro*, recombinant and mature MDA1 (rMDA1) was expressed in *E. coli* and affinity purified (Fig. 8a). rMDA1 has a predicted molecular weight of ~51 kDa but eluted from a size exclusion chromatography column at a size of ~100 kDa suggesting that it can form homodimers. rMDA1 containing fractions were pooled and the protein purity was confirmed by SDS-PAGE analysis (Fig. 8b). To test the affinity of rMDA1 for nucleic acids, gel mobility shift assays (GMS) were performed in absence of competitors using a synthetic 43-mer oligonucleotide probe in the form of ssDNA, dsDNA, ssRNA or dsRNA (Fig. 8c). rMDA1 did virtually not bind to dsRNA or ssDNA but showed clear binding to ssRNA and dsDNA with a more pronounced affinity for dsDNA. Thus, rMDA1 has the capacity to bind dsDNA and to lesser extent, ssRNA.

In order to test whether these properties applied *in vivo*, RIP-seq experiments on solubilized chloroplasts isolated from complemented plants were conducted but the results did not show substantial RNA enrichment in the immunoprecipitated samples when compared to the control (data not shown). This result indicates that MDA1 is not associated to RNA *in vivo*. We showed that MDA1 is required for the accumulation of transcripts whose processed forms are likely stabilized by PPR RNA binding protein caps (Fig. 4 and 5) (Ruwe *et al.*, 2016). To rule out the direct implication of MDA1 in this RNA stabilization process, additional GMS assays were performed using synthetic RNAs whose sequences correspond to the sRNAs matching processed 5'-ends of *ndhA* and *psbE* mRNAs or 3'-ends of *ndhA and psbJ* mRNAs (Fig. S4). In agreement with RIP-seq results, rMDA1 did not bind to any of these sRNAs (Fig. S5). Based on these *in vivo* and *in vitro* data, we concluded that MDA1 is not the RNA binding protein stabilizing the termini of mature *psbE-F-L-J* and *ndhA* containing mRNAs.

In a second step, we performed DIP-qPCR on solubilized chloroplasts and DNA enrichment for several genes in the *psbE* and *ndhH* operons was analyzed in the immunoprecipitated samples (Fig. 9). The results showed specific and significant DNA recovery for *psbE* and *ndhA* genes with a more pronounced enrichment in regions near their putative promoter (Fig. 9b). Moreover, we observed that the degree of enrichment for *psbE* was higher than that of *ndhA* indicating that MDA1 has a higher affinity for *psbE in vivo*. Taken together,

these results demonstrate that MDA1 binds specifically to DNA regions in *psbE* and *ndhA* genes whose transcript accumulation is impaired in *mda1* mutants.

MDA1 binds with specificity to 27-nt DNA sequences located near *psbE* and *ndhA* promoter regions

To prove direct MDA1 binding to its *in vivo* target genes and define the DNA segments that are necessary for interaction, we assayed rMDA1 *in vitro* binding to overlapping DNA segments derived from 230- or 330-bp regions covering respectively the *psbE* and *ndhA* putative promoters with regions near the 5'-end of their ORFs (Fig. 10). rMDA1 bound with high affinity and specificity to a 100-nt DNA segment, named E2 located upstream *psbE* (-125 to -26 bp from the ATG) and downstream the -127 PEP TSS (compare E2 to E1 and E3) (Fig. 10a). To precisely map the protein binding site, a DNase I footprint assay was conducted using the E2 DNA fragment in the presence or absence of rMDA1 (Fig. S6). rMDA1 protected a 27-bp DNA region from enzymatic cleavage mapping at position -96/-70 from the *psbE* ATG. MDA1 binding specificity to this genomic region was further tested in GMS assays using a 27-bp DNA fragment corresponding to the DNase-protected sequence (E4) or a DNA fragment of identical size mapping right downstream (E5). rMDA1 only bound the E4 segment demonstrating that the -96/-70 DNA region of the *psbE* gene is the putative MDA1 binding site.

MDA1 also acts on the *ndhA* locus *in vivo*. We showed that rMDA1 bound with specificity to a 130-bp *ndhA* DNA segment (A3) mapping +42/+171 within *ndhA* ORF (compare probe A3 to A1 and A2) (Fig. 10b). However, the affinity of rMDA1 for the *ndhA3* binding site was weaker than for the *psbE2* site as seen by the comparison of the amount of bound DNA at similar protein concentrations for each site. Contrary to *psbE2*, DNase footprinting performed with the *ndhA3* fragment did not lead to significant cleavage protection probably due to the lower affinity of rMDA1 for the *ndhA3* segment (data not shown). Thus, GMS assays were performed to delineate more precisely MDA1 binding sites using a series of shorter overlapping DNA fragments (from 60 to 27-bp size) spanning the *ndhA3* segment (probes A4 to A10). The results indicate that rMDA1 bound a 27-bp region located +110/+136 within the *ndhA ORF* (probe A10). Altogether, the GMS assay results showed that MDA1 binds with specificity to two DNA sequences located near the 5'-end of *psbE* and *ndhA* genes.

In agreement with MDA1 binding sites, our molecular analyses revealed that only a subset of chloroplast genes cotranscribed with *psbE* and *ndhA* is affected in *mda*1 mutants. We reasoned

that the two MDA1 binding sites in *psbE* and *ndhA* genes should therefore contain sufficient nucleotide conservation to define DNA specificity among the entire chloroplast genome. The alignment between the 27-bp *psbE* and *ndhA* binding sites revealed 10 conserved residues scattered along these sequences (Fig. 10c). This consensus sequence was matched against the entire Arabidopsis chloroplast genome to reveal 3 hits: the *psbE4* and *ndhA10* sites and an additional site in the *ndhD* gene. The DIP-qPCR analysis did not reveal any MDA1 *in vivo* association with *ndhD* gene and the expression of *ndhD* was unaffected in *mda1* mutants. These observations suggest that the two binding sites carry sufficient base conservation to define DNA specificity among the entire chloroplast genome but MDA1 might recognize additional elements to define its physiologically relevant gene targets *in vivo*.

Discussion

In this study, we have demonstrated novel aspects to the function of MDA1 in Arabidopsis, also known as mTERF5 (Ding *et al.*, 2019). Similar to our results, Ding *et al.* showed that mTERF5/MDA1 is required for the accumulation of *psbE-F-L-J* mRNA in chloroplasts and positively regulates transcription at the *psbE* promoter. Consistent with our findings, they showed that mTERF5 bound *in vitro* and *in vivo* to a DNA sequence near the *psbE* promoter that maps to our MDA1 footprint and, demonstrated that this binding site contains a transcription pausing site. Finally, they revealed that mTERF5 associates *in vivo* with the plastid TAC component, pTAC6 and that this interaction allows the recruitment of the PEP complex near the *psbE* promoter to pause gene transcription *in vivo*. However, their functional model for mTERF5/MDA1 did not explain how the lack of transcription pausing at the *psbE* promoter causes the severe loss of the *psbE-F-L-J* mRNA in the *mterf5/mda1* mutant, particularly, when considering that the transcription activity at *psbE* is only partially reduced in the *mterf5*/*mda1* mutant compared to wild-type (Fig. 6). Our study showed that MDA1/mTERF5 had an additional *in vivo* gene target in the *ndhH* operon. We demonstrated that MDA1 was additionally required for the accumulation of specific *ndhA-I* mRNAs and importantly, that the *psbE* and *ndhA* containing mRNAs that require MDA1 for their *in vivo* accumulation result from posttranscriptional RNA processing most likely involving the participation of exoribonucleases with PPR RNA binding proteins that protect and stabilize the processed mRNA ends. The analysis of the accumulation of the sRNA PPR footprints in *mda1* indicated that MDA1 specifically promotes the *in vivo* binding of an RNA binding protein (presumably a PPR protein) to the 5'-end of the processed *psbE* and *ndhA* mRNAs. On contrary to

Ding *et al.*, our MDA1 coimmunoprecipitation analysis revealed that MDA1 associates *in vivo* not only with pTAC6 but many TAC components, including the PEP core subunits. Finally, the relative quantification of the transcription activity at *psbE* and *ndhA* demonstrated that their reduction in *mda1* could not justify in itself the more severe loss of their processed mRNAs in the mutant. Altogether, our results demonstrated that MDA1/mTERF5 functions not only in stimulating transcription of *psbE* and *ndhA* genes but also in the stabilization of their posttranscriptionally processed mRNAs. A potential functional model for MDA1 explaining its dual contribution to gene transcription and RNA stabilization in chloroplasts is discussed below.

MDA1: linking transcription and RNA stabilization of its target genes

MDA1 promotes both transcription of *psbE* and *ndhA* gene and the stabilization of their 5'-end processed mRNAs. Our coIP results suggest that MDA1 interacts *in vivo* with the PEP transcription complex. Thus, the specific DNA binding of MDA1 near the *psbE* promoter most likely induces recruitment of components of the PEP complex to stimulate gene transcription locally. A puzzling question is how the DNA binding protein, MDA1 additionally promotes the stabilization of the processed 5'-end of *psbE* and *ndhA* RNAs. Answers to this question might come from the analysis of the genomic location of the MDA1 binding site in *psbE* (Fig. 11a). MDA1 binding site is placed 29 nucleotides downstream the position of the 5'-end of processed *psbE* RNA and this binding site coincides with a transcriptional pausing site identified by Ding *et al.* whose *in vivo* activity requires MDA1 (Ding *et al.*, 2019). The 29-nt region directly upstream of this transcriptional pausing site matches the sequence of the sRNA that is bound *in vivo* by an unknown PPR-like RNA binding protein that stabilizes the 5'-end of processed *psbE* mRNA that is missing in *mda1*. The stability of *psbE* mRNA depends on the capacity of this RNA binding protein to bind its RNA target. Biochemical studies have shown that PPR proteins preferentially bind single-stranded RNA whereas their capacity to invade RNA secondary structures is very limited (Williams-Carrier *et al.*, 2008; Hammani *et al.*, 2011; McDermott *et al.*, 2018). Therefore, *in vivo* mechanisms should exist to facilitate PPR binding to their RNA target sequences when these are folded in secondary structures (Jiang *et al.*, 2019). A transcriptional pausing site strategically placed downstream of a PPR binding site offers an attractive mechanism by which to pause RNA elongation and preclude the formation of secondary structures that would otherwise be deleterious for PPR binding and RNA stabilization. We used the mfold server (Zuker, 2003) to predict RNA structures of neotranscribed *psbE* RNA segments including or excluding pausing at

the MDA1 binding site (Fig. 11b). As expected, when transcription is paused at this site by MDA1, the 5'-end of the *psbE* RNA and the PPR binding site do not fold into a stable RNA structure (d*G* > -5 kcal/mol) and would allow PPR binding and the subsequent *psbE* mRNA stabilization. On the contrary, farther RNA elongation to the MDA1 binding site or the *psbE* start codon are predicted to allow the formation of stable RNA-RNA interactions (d*G* < -10 kcal/mol) that occlude the PPR binding site and presumably compete with the PPR binding. Based on this observation and our experimental results, we hypothesize that MDA1 promotes *psbE* mRNA stability by pausing gene transcription to facilitate binding of a PPR protein to the RNA 5'-end which in turn, stabilizes the mRNA *in vivo*.

The MDA1 binding site in *ndhA* is located in the first exon and farther downstream from the gene promoter than for *psbE.* Although a transcriptional pausing site has not been clearly identified in *ndhA* by Ding *et al.*, the *ndhA* 5' sRNA PPR footprint is specifically missing in *mda1*. This suggests that MDA1 might execute an analogous function at this site to cooperate with an RNA binding protein that stabilizes the 5'-end of *ndhA* RNA *in vivo*.

Altogether, our results reveal the importance of DNA binding proteins in the regulation of posttranscriptional processes in chloroplasts. Molecular and biochemical studies of the uncharacterized *mTERF* genes in plants will likely lead to the discovery of new regulatory mechanisms in chloroplast gene expression and a better understanding of the interplay between DNA and RNA metabolism in chloroplasts.

Acknowledgments

The authors thank Alice Barkan and Rosalind William-Carrier (University of Oregon) for performing the RIP-seq analysis. This study was supported by a grant from Agence Nationale de la Recherche (ANR-16-CE20-0007) to KH, the DFG (ZO 302/5-1) to RZ and the SFB-TRR175 to JM (A03) and RZ (A04).

Author Contributions

KH, RZ, L-VM and RG designed the research. L-VM, RG, KM, KH, AZ, JC, AA, NB and JM performed research. KH and L-VM wrote the manuscript and RZ, RG and JM edited it.

References

Allorent G, Courtois F, Chevalier F, Lerbs-Mache S. 2013. Plastid gene expression during chloroplast differentiation and dedifferentiation into non-photosynthetic plastids during seed formation. *Plant Mol Biol* **82**(1-2): 59-70.

Babiychuk E, Vandepoele K, Wissing J, Garcia-Diaz M, De Rycke R, Akbari H, Joubes J, Beeckman T, Jansch L, Frentzen M, et al. 2011. Plastid gene expression and plant development require a plastidic protein of the mitochondrial transcription termination factor family. *Proc Natl Acad Sci U S A* **108**(16): 6674-6679.

Barkan A. 1998. Approaches to investigating nuclear genes that function in chloroplast biogenesis in land plants. *Photosynthesis: Molecular Biology of Energy Capture* **297**: 38-57.

Barkan A. 2011. Expression of plastid genes: organelle-specific elaborations on a prokaryotic scaffold. *Plant Physiol* **155**(4): 1520-1532.

Berglund AK, Pujol C, Duchene AM, Glaser E. 2009. Defining the determinants for dual targeting of amino acyl-tRNA synthetases to mitochondria and chloroplasts. *J Mol Biol* **393**(4): 803-814.

Castandet B, Germain A, Hotto AM, Stern DB. 2019. Systematic sequencing of chloroplast transcript termini from Arabidopsis *thaliana* reveals >200 transcription initiation sites and the extensive imprints of RNA-binding proteins and secondary structures. *Nucleic Acids Res* **47**(22): 11889-11905.

Ding S, Zhang Y, Hu Z, Huang X, Zhang B, Lu Q, Wen X, Wang Y, Lu C. 2019. mTERF5 Acts as a Transcriptional Pausing Factor to Positively Regulate Transcription of Chloroplast *psbEFLJ*. *Mol Plant* **12**(9): 1259-1277.

Fujiki Y, Hubbard AL, Fowler S, Lazarow PB. 1982. Isolation of intracellular membranes by means of sodium carbonate treatment: application to endoplasmic reticulum. *J Cell Biol* **93**(1): 97-102.

Hammani K, Barkan A. 2014. An mTERF domain protein functions in group II intron splicing in maize chloroplasts. *Nucleic Acids Res* **42**(8): 5033-5042.

Hammani K, Bonnard G, Bouchoucha A, Gobert A, Pinker F, Salinas T, Giege P. 2014. Helical repeats modular proteins are major players for organelle gene expression. *Biochimie* **100C**: 141-150.

Hammani K, des Francs-Small CC, Takenaka M, Tanz SK, Okuda K, Shikanai T, Brennicke A, Small I. 2011. The pentatricopeptide repeat protein OTP87 is essential for

RNA editing of *nad7* and *atp1* transcripts in Arabidopsis mitochondria. *J Biol Chem* **286**(24): 21361-21371.

Hsu YW, Wang HJ, Hsieh MH, Hsieh HL, Jauh GY. 2014. Arabidopsis mTERF15 is required for mitochondrial *nad2* intron 3 splicing and functional complex I activity. *PLoS One* **9**(11): e112360.

Jiang J, Chai X, Manavski N, Williams-Carrier R, He B, Brachmann A, Ji D, Ouyang M, Liu Y, Barkan A, et al. 2019. An RNA Chaperone-Like Protein Plays Critical Roles in Chloroplast mRNA Stability and Translation in Arabidopsis and Maize. *Plant Cell* **31**(6): 1308-1327.

Jimenez-Menendez N, Fernandez-Millan P, Rubio-Cosials A, Arnan C, Montoya J, Jacobs HT, Bernado P, Coll M, Uson I, Sola M. 2010. Human mitochondrial mTERF wraps around DNA through a left-handed superhelical tandem repeat. *Nat Struct Mol Biol* **17**(7): 891-893.

Kleine T. 2012. Arabidopsis *thaliana* mTERF proteins: evolution and functional classification. *Front Plant Sci* **3**: 233.

Kleine T, Leister D. 2015. Emerging functions of mammalian and plant mTERFs. *Biochim Biophys Acta* **1847**(9): 786-797.

Kleinknecht L, Wang F, Stube R, Philippar K, Nickelsen J, Bohne AV. 2014. RAP, the sole octotricopeptide repeat protein in Arabidopsis, is required for chloroplast 16S rRNA maturation. *Plant Cell* **26**(2): 777-787.

Kunst L. 1998. Preparation of physiologically active chloroplasts from Arabidopsis. *Methods Mol Biol* **82**: 43-48.

Lange H, Ndecky SYA, Gomez-Diaz C, Pflieger D, Butel N, Zumsteg J, Kuhn L, Piermaria C, Chicher J, Christie M, et al. 2019. RST1 and RIPR connect the cytosolic RNA exosome to the Ski complex in Arabidopsis. *Nat Commun* **10**(1): 3871.

Lu C, Meyers BC, Green PJ. 2007. Construction of small RNA cDNA libraries for deep sequencing. *Methods* **43**(2): 110-117.

Maria del Campo E, Sabater B, Martin M. 2006. Characterization of the 5'- and 3'-ends of mRNAs of ndhH, ndhA and ndhI genes of the plastid *ndhH-D* operon. *Biochimie* **88**(3-4): 347-357.

McDermott JJ, Civic B, Barkan A. 2018. Effects of RNA structure and salt concentration on the affinity and kinetics of interactions between pentatricopeptide repeat proteins and their RNA ligands. *PLoS One* **13**(12): e0209713.

Meurer J, Meierhoff K, Westhoff P. 1996. Isolation of high-chlorophyll-fluorescence mutants of *Arabidopsis thaliana* and their characterisation by spectroscopy, immunoblotting and northern hybridisation. *Planta* **198**(3): 385-396.

Nunez-Delegido E, Robles P, Ferrandez-Ayela A, Quesada V. 2019. Functional analysis of mTERF5 and mTERF9 contribution to salt tolerance, plastid gene expression and retrograde signalling in *Arabidopsis thaliana*. *Plant Biol (Stuttg)* **DOI**: 10.1111/plb.13084.

Pfalz J, Liere K, Kandlbinder A, Dietz KJ, Oelmuller R. 2006. pTAC2, -6, and -12 are components of the transcriptionally active plastid chromosome that are required for plastid gene expression. *Plant Cell* **18**(1): 176-197.

Roberti M, Polosa PL, Bruni F, Manzari C, Deceglie S, Gadaleta MN, Cantatore P. 2009. The MTERF family proteins: mitochondrial transcription regulators and beyond. *Biochim Biophys Acta* **1787**(5): 303-311.

Robles P, Micol JL, Quesada V. 2012. Arabidopsis MDA1, a nuclear-encoded protein, functions in chloroplast development and abiotic stress responses. *PLoS One* **7**(8): e42924.

Robles P, Navarro-Cartagena S, Ferrandez-Ayela A, Nunez-Delegido E, Quesada V. 2018. The Characterization of Arabidopsis mterf6 Mutants Reveals a New Role for mTERF6 in Tolerance to Abiotic Stress. *Int J Mol Sci* **19**(8): 2388.

Romani I, Manavski N, Morosetti A, Tadini L, Maier S, Kuhn K, Ruwe H, Schmitz-Linneweber C, Wanner G, Leister D, et al. 2015. A Member of the Arabidopsis Mitochondrial Transcription Termination Factor Family Is Required for Maturation of Chloroplast Transfer RNA*Ile(GAU)*. *Plant Physiol* **169**(1): 627-646.

Ruwe H, Schmitz-Linneweber C. 2012. Short non-coding RNA fragments accumulating in chloroplasts: footprints of RNA binding proteins? *Nucleic Acids Res* **40**(7): 3106-3116.

Ruwe H, Wang G, Gusewski S, Schmitz-Linneweber C. 2016. Systematic analysis of plant mitochondrial and chloroplast small RNAs suggests organelle-specific mRNA stabilization mechanisms. *Nucleic Acids Res* **44**(15): 7406-7417.

Saleh A, Alvarez-Venegas R, Avramova Z. 2008. An efficient chromatin immunoprecipitation (ChIP) protocol for studying histone modifications in Arabidopsis plants. *Nat Protoc* **3**(6): 1018-1025.

Sane AP, Stein B, Westhoff P. 2005. The nuclear gene HCF107 encodes a membrane-associated R-TPR (RNA tetratricopeptide repeat)-containing protein involved in expression of the plastidial *psbH* gene in Arabidopsis. *Plant J* **42**(5): 720-730.

Sato N, Terasawa K, Miyajima K, Kabeya Y. 2003. Organization, developmental dynamics, and evolution of plastid nucleoids. *Int Rev Cytol* **232**: 217-262.

Sato S, Nakamura Y, Kaneko T, Asamizu E, Tabata S. 1999. Complete structure of the chloroplast genome of Arabidopsis *thaliana*. *DNA Res* **6**(5): 283-290.

Swiatek M, Regel RE, Meurer J, Wanner G, Pakrasi HB, Ohad I, Herrmann RG. 2003. Effects of selective inactivation of individual genes for low-molecular-mass subunits on the assembly of photosystem II, as revealed by chloroplast transformation: the psbEFLJoperon in Nicotiana tabacum. *Mol Genet Genomics* **268**(6): 699-710.

Torabi S, Umate P, Manavski N, Plochinger M, Kleinknecht L, Bogireddi H, Herrmann RG, Wanner G, Schroder WP, Meurer J. 2014. PsbN is required for assembly of the photosystem II reaction center in Nicotiana tabacum. *Plant Cell* **26**(3): 1183-1199.

Westhoff P, Alt J, Widger WR, Cramer WA, Herrmann RG. 1985. Localization of the gene for apocytochromeb-559 on the plastid chromosome of spinach. *Plant Mol Biol* **4**(2-3): 103-110.

Williams-Carrier R, Kroeger T, Barkan A. 2008. Sequence-specific binding of a chloroplast pentatricopeptide repeat protein to its native group II intron ligand. *RNA* **14**(9): 1930-1941.

Xiong HB, Wang J, Huang C, Rochaix JD, Lin FM, Zhang JX, Ye LS, Shi XH, Yu QB, Yang ZN. 2020. mTERF8, a Member of the Mitochondrial Transcription Termination Factor Family, is Involved in the Transcription Termination of Chloroplast Gene *psbJ1*. *Plant Physiol* **182**(1): 408-423.

Xu D, Leister D, Kleine T. 2017. Arabidopsis *thaliana* mTERF10 and mTERF11, but Not mTERF12, Are Involved in the Response to Salt Stress. *Front Plant Sci* **8**: 1213.

Yakubovskaya E, Mejia E, Byrnes J, Hambardjieva E, Garcia-Diaz M. 2010. Helix unwinding and base flipping enable human MTERF1 to terminate mitochondrial transcription. *Cell* **141**(6): 982-993.

Zhang Y, Cui YL, Zhang XL, Yu QB, Wang X, Yuan XB, Qin XM, He XF, Huang C, Yang ZN. 2018. A nuclear-encoded protein, mTERF6, mediates transcription termination of *rpoA* polycistron for plastid-encoded RNA polymerase-dependent chloroplast gene expression and chloroplast development. *Sci Rep* **8**(1): 11929.

Zhao Y, Cai M, Zhang X, Li Y, Zhang J, Zhao H, Kong F, Zheng Y, Qiu F. 2014. Genome-wide identification, evolution and expression analysis of mTERF gene family in maize. *PLoS One* **9**(4): e94126.

Zhelyazkova P, Hammani K, Rojas M, Voelker R, Vargas-Suarez M, Borner T, Barkan A. 2012. Protein-mediated protection as the predominant mechanism for defining processed mRNA termini in land plant chloroplasts. *Nucleic Acids Res* **40**(7): 3092-3105.

Zhou B, Zhang L, Ullah A, Jin X, Yang X, Zhang X. 2016. Identification of Multiple Stress Responsive Genes by Sequencing a Normalized cDNA Library from Sea-Land Cotton (*Gossypium barbadense* L.). *PLoS One* **11**(3): e0152927.

Zoschke R, Watkins KP, Barkan A. 2013. A rapid ribosome profiling method elucidates chloroplast ribosome behavior *in vivo*. *Plant Cell* **25**(6): 2265-2275.

Zubo YO, Borner T, Liere K. 2011. Measurement of transcription rates in Arabidopsis chloroplasts. *Methods Mol Biol* **774**: 171-182.

Zuker M. 2003. Mfold web server for nucleic acid folding and hybridization prediction. *Nucleic Acids Res* **31**(13): 3406-3415.

Figure legends

Fig. 1 Characterization of *mda1* mutant plants in Arabidopsis. (a) Schematic representations of the *MDA1* gene and protein with the locations of mutant alleles used in this study. TP: putative chloroplast transit peptide. (b) Phenotypes of wild-type (WT), *mda1-2* mutant and complemented (CP) plants grown in medium or soil at several developmental stages. (c) RT-PCR analysis of *mda1* gene expression in wild-type, *mda1-2* and CP plants. Genomic DNA (gDNA) template was used as a PCR positive control and *ACTIN-2* gene (*ACT2*) serves as the internal RT-PCR control. (d) Transient coexpression assay of MDA1-GFP and RAP-RFP fusion proteins in tobacco protoplasts. Fluorescence images of GFP, RFP, chlorophyll as well as a merged image are shown. Magnified views of the region delineated by a white box are provided below.

Fig. 2 Immunodetection analyses of chloroplast proteins in Arabidopsis WT, *mda1-2* and complemented plants (CP). Replicate immunoblots of total leaf protein extract were probed with antibodies targeted against subunits of the chloroplast photosystem II (PSII: PsbD, PsbH, PsbE), photosystem I (PsaD), NADH dehydrogenase (NDH: NdhB, NdhL), cytochrome b_6f (PetD), ATP

synthase (AtpA), Rubisco (RbcL) and ribosome (Rps1) complexes. One of the replicate membranes was stained with Coomassie Blue (CBB) to show equal protein loading.

Fig. 3 Steady state levels of chloroplast gene transcripts in Arabidopsis *mda1*. Transcript levels were determined by qRT-PCR and are displayed as the $\log_2$ fold change (FC) between values obtained for the mutant or the complemented plants and the wild-type plants. Genes are ordered according to their genome positions. The nuclear *ACT2* and *TIP41* genes were used for data normalization. The values from two biological replicates performed each with technical triplicate were averaged per genotype and standard errors are indicated.

Fig. 4 RNA gel blot analyses of transcripts of the Arabidopsis *psbE* and *ndhH* operons. (a) Genetic map of the *psbE* gene cluster indicating the positions of TSS (right squared arrows) and mapped transcript termini (circle arrow tips). Positions are specified relative to gene start or stop codon. Black circle arrow tips indicate transcript termini whose positions coincide with the presence of an abundant sRNA in chloroplasts whose sequences are given in Fig. S4. (b) Replicate blots of WT, *mda1-2* and CP RNA were hybridized with 60-mer oligonucleotides strand specific probes whose positions are indicated beneath the map in (a). The methylene blue stained blots are shown to illustrate equal loading of rRNAs. Transcripts whose positions could be assigned from these results are diagrammed below the map and their length is given in kilobases (kb). (c) Mapping of transcript ends for *psbE-F-J-L* genes in different genotypes by cRT-PCR. Primers used for PCR are indicated on the right and displayed on the map. The numbers of clones with the specified ends are indicated in the table. The RNA sequences of the predominant 5' and 3'-ends and the sRNAs are provided in Fig. S4. (d) Genetic map of the *ndhA* gene cluster. (e) RNA blots hybridized with strand specific probes. (f) Mapping of transcript ends for *ndhA* gene by cRT-PCR.

Fig. 5 RNA gel blot analyses of chloroplast sRNAs accumulation in Arabidopsis *mda1*. Five μg of low-molecular-weight leaf RNA (or 10 μg for *psbJ* and *ndhA* 3') of the indicated genotypes was fractionated in denaturing polyacrylamide gels and transferred to nylon membrane. Blots were hybridized with oligonucleotide probes complementary to sequences of sRNAs accumulating in the chloroplast regions listed on the right. The accumulation of two sRNAs matching the 5'-end of *psaC* or *rbcL* mRNAs whose RNA abundance are unaffected in *mda1* were monitored as internal

controls. A portion of one of the gels stained by ethidium bromide (EtBr) is shown below to illustrate equal loading.

Fig. 6 Run-on transcription assay of chloroplast genes in Arabidopsis *mda1*. (a) Slot-blot analysis of run-on transcript samples from chloroplasts of the indicated genotypes hybridized to DNA fragments representing chloroplast *rrn16*, *ndhH*, *ndhA, psaC* and *psbE* genes. (b) Percent changes relative to WT of run-on transcription rates, the mRNA steady state levels measured by qRT-PCR or/and RNA gel blot analyses. *rrn16* was used as reference gene for the normalization of transcription rates. The quantification of mRNAs from RNA gel blots was performed on mature 1.1 kb *psbE-F-L-J* and 0.5 kb monocistronic *psaC* mRNAs. Data are means of three independent experiments and standard errors are indicated.

Fig. 7 Arabidopsis MDA1 is found in high-molecular-weight complexes *in vivo* and associates with PEP and TAC components. (a) MDA1 is a peripheral membrane protein whose membrane association is RNA and DNA-independent. Chloroplast membrane fractions (C) were mock-treated or 0.2 M Na_2CO_3, RNase, DNase, 1% NP40 treated before centrifugation. The presence of MDA1 in the pellet (P) or soluble fraction (S) after treatment was analyzed by immunoblotting with an antibody against the Myc epitope or the chloroplast integral membrane protein, PsaD as a control. The membrane stained with Coomassie Blue (CBB) is shown below. (b) Sucrose gradient fractionation of mock, RNase and DNase treated chloroplast extracts. An equal volume of each fraction was analyzed on immunoblots using antibodies indicated at left. The chloroplast RNA intron splicing factor proteins, mTERF4 and the ribosomal protein Rpl33 are found in high-molecular weight complexes of ~0.55 MDa and 1 MDa, respectively (Hammani & Barkan, 2014) and serve as size fractionation controls. (c) Chloroplast protein interactome of MDA1. MDA1 coimmunoprecipitates (coIP) with components of the plastid TAC (Pfalz *et al.*, 2006) including the subunits of the plastid encoded RNA polymerase. Solubilized chloroplasts from complemented *mda1* plants expressing the 4Myc-tagged MDA1 (CP) or WT plants were used for immunoprecipitation with anti-Myc antibody and, coIP proteins were identified by MS analysis. Volcano plots show the enrichment of proteins copurified with 4Myc-tagged MDA1 as compared with control IPs. IPs were performed on biological triplicate. Y- and X-axes display the negative common logarithm of the adjusted false discovery rate (FDR) and fold changes, respectively. The dashed lines indicate the threshold above which proteins are significantly enriched (FDR <0.05

and FC >4). TAC components (Pfalz *et al.*, 2006) are represented as green dots. The immunoblot validation of RpoB association is shown. Replicate immunoblots were probed with anti-Myc or RpoB antibody. The full list of MDA1-associated proteins is available in Table S4.

Fig. 8 Recombinant Arabidopsis MDA1 binds ssRNA and dsDNA *in vitro*. (a) Purification of recombinant MDA1 (rMDA1). rMDA1 was expressed as maltose binding protein (MBP) fusion and purified by amylose affinity chromatography. After TEV cleavage free rMDA1 and MBP were resolved by gel filtration (FPLC). Aliquots of column fractions were analyzed by SDS/PAGE and stained with Coomassie Blue. The elution positions of rMDA1 (~100 kDa) and the Conalbumine (77 kDa) and Ovalbumine (44 kDa) molecular weight (MW) markers are indicated below the gel. (b) SDS/PAGE analysis of the purity of the final rMDA1 used for *in vitro* assays. (c) Gel mobility shift assays showing ssRNA and dsDNA binding of rMDA1. Increasing amounts of rMDA1 (0, 50, 100 and 200 nM) were incubated with synthetic 43-mer RNA or DNA oligonucleotides of the same random sequence in single- or double-stranded forms and resolved on a native polyacrylamide gel. Free nucleic acids migrate to the bottom of the gel whereas rMDA1-nucleic acid complexes are shifted up on the gel and are indicated by white diamonds.

Fig. 9 Arabidopsis chloroplast DNA immunoprecipitation quantitative PCR (DIP-qPCR) analysis of MDA1 DNA binding activity *in vivo*. (a) Immunoprecipitation efficiency of 4Myc-tagged MDA1 on chloroplasts extracted from complemented *mda1* plants (CP). WT chloroplasts were used as input for negative experimental controls. A fraction of the input (Tot), supernatant (Sup) and pellet (Pel) samples were analyzed on immunoblots by probing with Myc antibodies. (b) Levels of immunoprecipitated DNA of various chloroplast DNA regions were calculated as percent recovery of the total input DNA. The significance of the variation between CP and control IPs were analyzed with a two-way ANOVA, Tukey's test. *Indicates P <0.05, ** <0.005, *** <0.0005 and **** <0.00005, ns: not significant. The DNA fold enrichment in CP IPs relative to WT is shown below. Data are means of three independent experiments and standard errors are indicated.

Fig. 10 Preferential DNA binding of rMDA1 to regions near the 5'-end of chloroplast *psbE* and *ndhA* Arabidopsis genes. (a) Gel mobility shift assays showing specific DNA binding of rMDA1 to a short DNA sequence upstream of *psbE* start codon. Different amounts of rMDA1 (0,

12.5, 25, 50 nM) were incubated with overlapping DNA segments of various sizes that span the -190/+40 genomic region from *psbE* start codon in the presence of poly(dI-dC) competitor. The length of the DNA fragments is given in base pairs on the left side. DNA fragment E2 was used for MDA1 DNase footprinting analysis shown in Fig S6. (b) Gel mobility shift assays showing specific DNA binding of rMDA1 to a DNA sequence downstream of *ndhA* start codon. Binding conditions were identical to those used in (a) and the DNA fragments covered a -159/+171 genomic region from the *ndhA* start codon. (c) Sequence alignment of the 27-bp *psbE* and *ndhA* MDA1 binding sites. Conserved bases are shaded in black and the consensus sequence is given below.

Fig. 11 Potential mechanism of MDA1 action on *psbE* 5' RNA stabilization in Arabidopsis. (a) Nucleotide sequence of the -161/+17 *psbE* genomic region. The genomic positions are given according to *psbE* start codon. The -35 and -10 consensus eubacterial (PEP) promoter elements, TSS (right squared arrow) and *in vivo* 5'-end of processed *psbE* mRNA (circled arrow tip) are positioned on the map. The sequences of the 5' *psbE* sRNA PPR footprint that is specifically lost in *mda1* and MDA1 DNA binding site are underlined by gray and blue arrows, respectively. The MDA1 binding site contains a transcription pausing site (Ding *et al.*, 2019). The 5' region of the *psbE* coding sequence is underlined by a yellow arrow. (b) Mfold prediction of the most stable structure of neotranscribed RNA sequences from *psbE* TSS (-127) to the PEP pausing site (-96) or farther downstream to the MDA1 binding site (-70) or upstream the *psbE* start codon (-1). The sequences of the 5' *psbE* sRNA and MDA1 footprint are underlined using the same color code as in (a). The calculated d*G* for each RNA structure is given in kcal/mol. MDA1 DNA binding downstream of the PPR footprint sequence pauses gene transcription and would prevent the folding of the footprint into a secondary RNA structure that is deleterious for the PPR binding to the 5' end of *psbE* mRNA and therefore, the post-transcriptional stabilization of the processed *psbE* mRNA *in vivo*.

Supporting Information

Additional supporting information may be found in the online version of this article.

Fig. S1. Phenotype and ribosome profiling analyses of the Arabidopsis *mda1* mutant allele *hcf111-1*.

Fig. S2. MDA1 is associated to membranes in chloroplasts.

Fig. S3. Quantification of the abundance of the 1.4 and 1.1 kb *psbE-F-L-J* mRNAs in the different plant genotypes by RNA blot analyses.

Fig. S4. Genome mapping of the predominant *in vivo* 5' and 3' ends for the processed *psbE-F-L-J* and *ndhA* mRNAs determined by cRT-PCR in different genotypes.

Fig. S5. RNA gel mobility shift assays showing no binding of MDA1 to sRNAs.

Fig. S6. *psbE* DNase footprinting assays.

Methods S1. Photosynthetic capacity measurements and genome wide analyses of chloroplast transcriptome and translatome.

Table S1. List of oligonucleotides used in this study.

Table S2. Chlorophyll *a* fluorescence induction and light-induced PSI absorbance changes.

Table S3. Ribosome profiling data of *hcf111-1*.

Table S4. List of proteins identified by LC-MS/MS in coimmunopurification assays using MDA1 as bait.

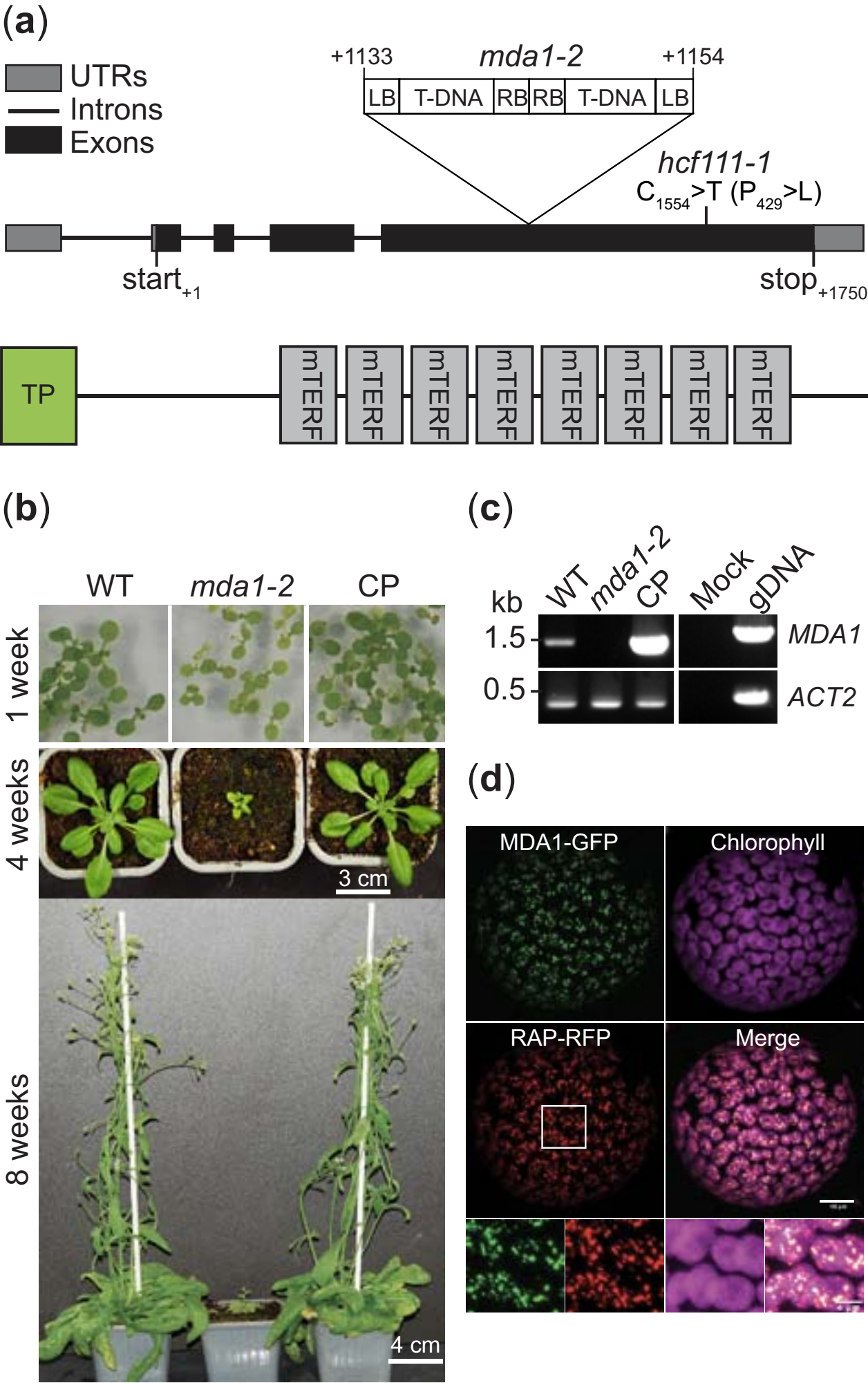
(a)
UTRs
Introns
Exons
+1133
mda1-2
+1154
LB
T-DNA
RB
RB
T-DNA
LB
hcf111-1
C1554>T (P429>L)
start+1
stop+1750
TP
mTERF
mTERF
mTERF
mTERF
mTERF
mTERF
mTERF
mTERF
(b)
WT
mda1-2
CP
1 week
4 weeks
8 weeks
3 cm
4 cm
(c)
kb
WT
mda1-2
CP
Mock
gDNA
1.5
0.5
MDA1
ACT2
(d)
MDA1-GFP
Chlorophyll
RAP-RFP
Merge

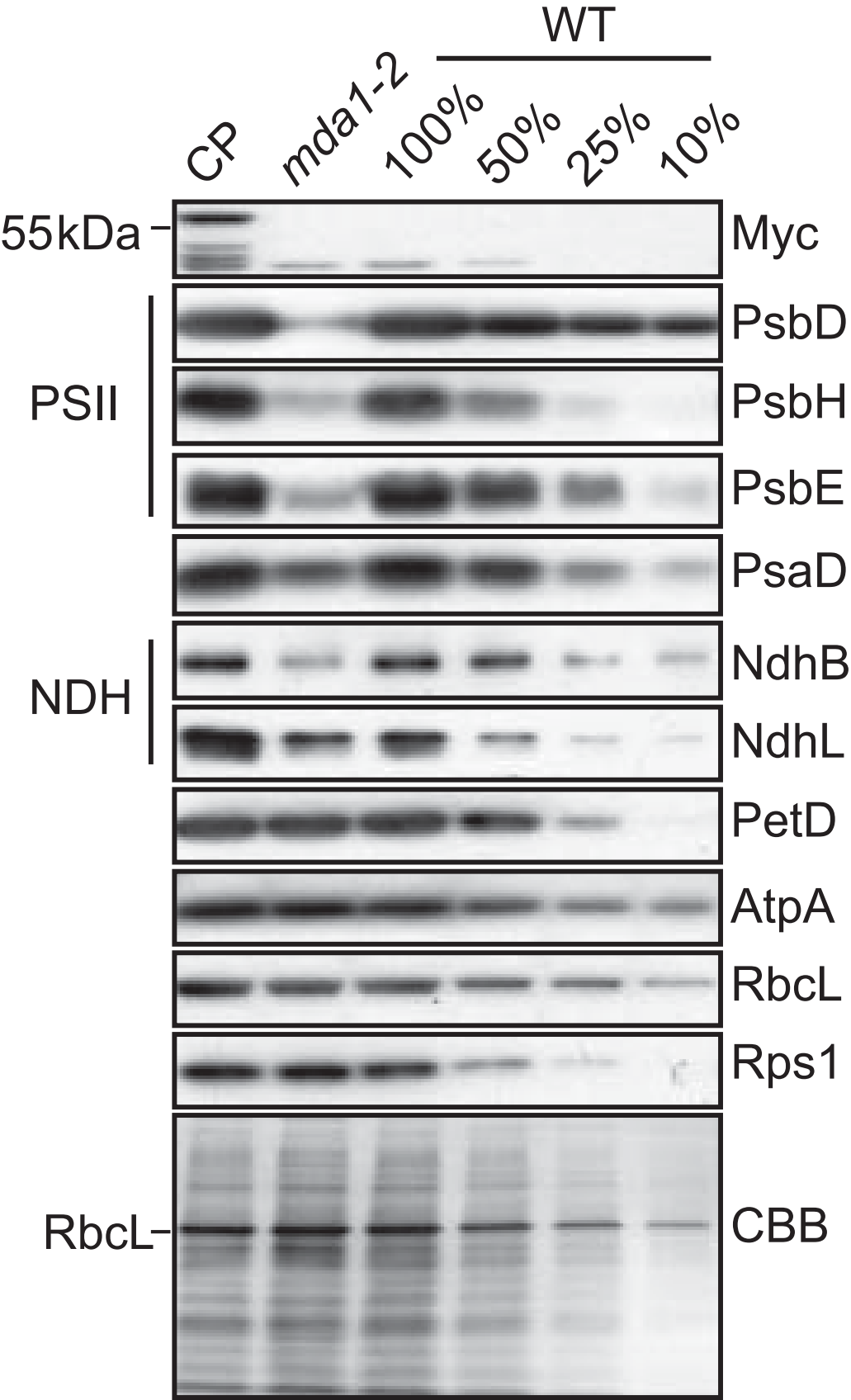
WT
CP
mda1-2
100%
50%
25%
10%
55kDa
Myc
PSII
PsbD
PsbH
PsbE
PsaD
NDH
NdhB
NdhL
PetD
AtpA
RbcL
Rps1
RbcL
CBB

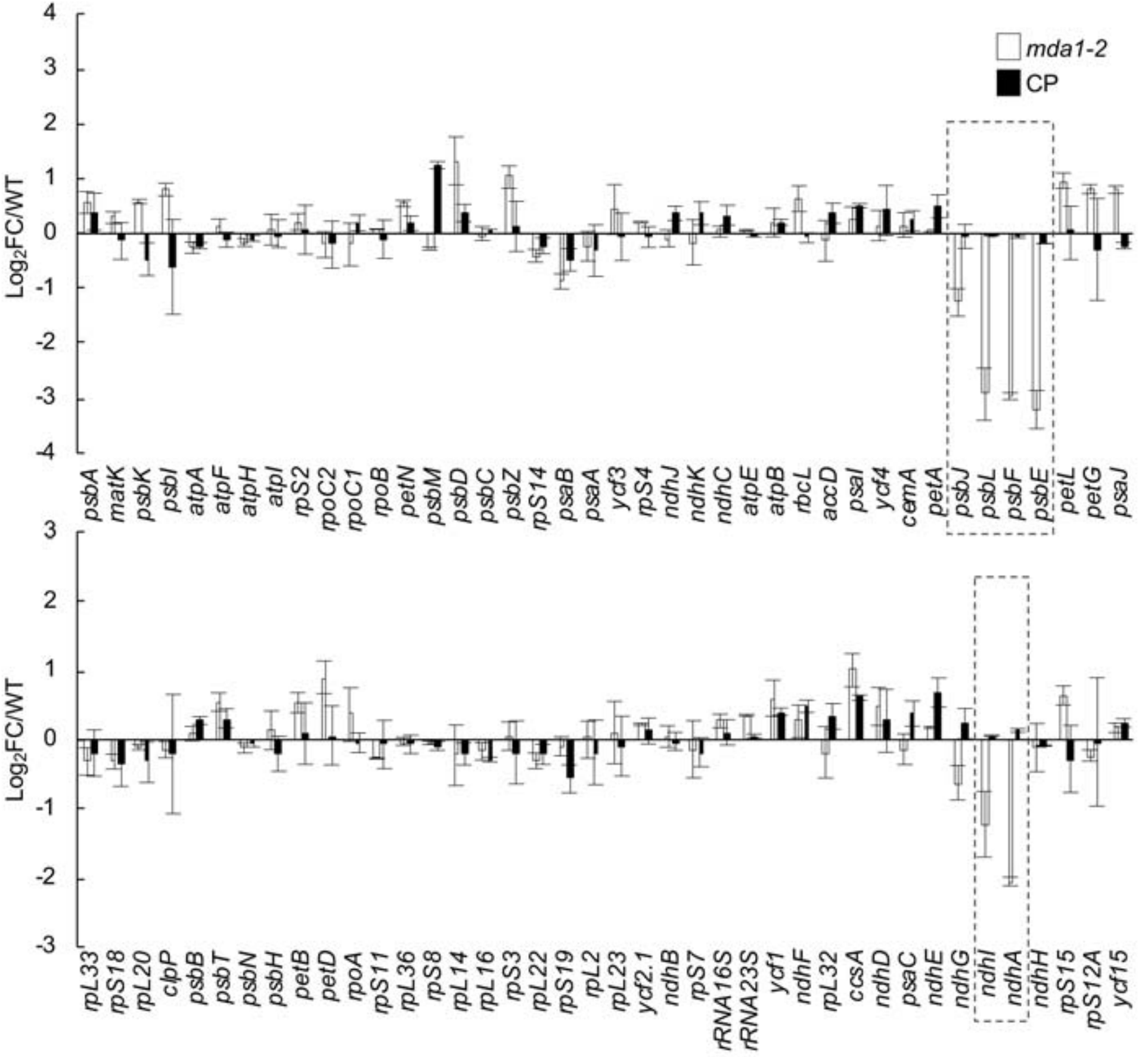
mda1-2
CP
Log2FC/WT
4
3
2
1
0
-1
-2
-3
-4
psbA matK psbK psbI atpA atpF atpH atpI rpS2 rpoC2 rpoC1 rpoB petN psbM psbD psbC psbZ rpS14 psaB psaA ycf3 rpS4 ndhJ ndhK ndhC atpE atpB rbcL accD psaI ycf4 cemA petA psbJ psbL psbF psbE petL petG psaJ
Log2FC/WT
3
2
1
0
-1
-2
-3
rpL33 rpS18 rpL20 clpP psbB psbT psbN psbH petB petD rpoA rpS11 rpL36 rpS8 rpL14 rpL16 rpS3 rpL22 rpS19 rpL2 rpL23 ycf2.1 ndhB rpS7 rRNA16S rRNA23S ycf1 ndhF rpL32 ccsA ndhD psaC ndhE ndhG ndhI ndhA ndhH rpS15 rpS12A ycf15

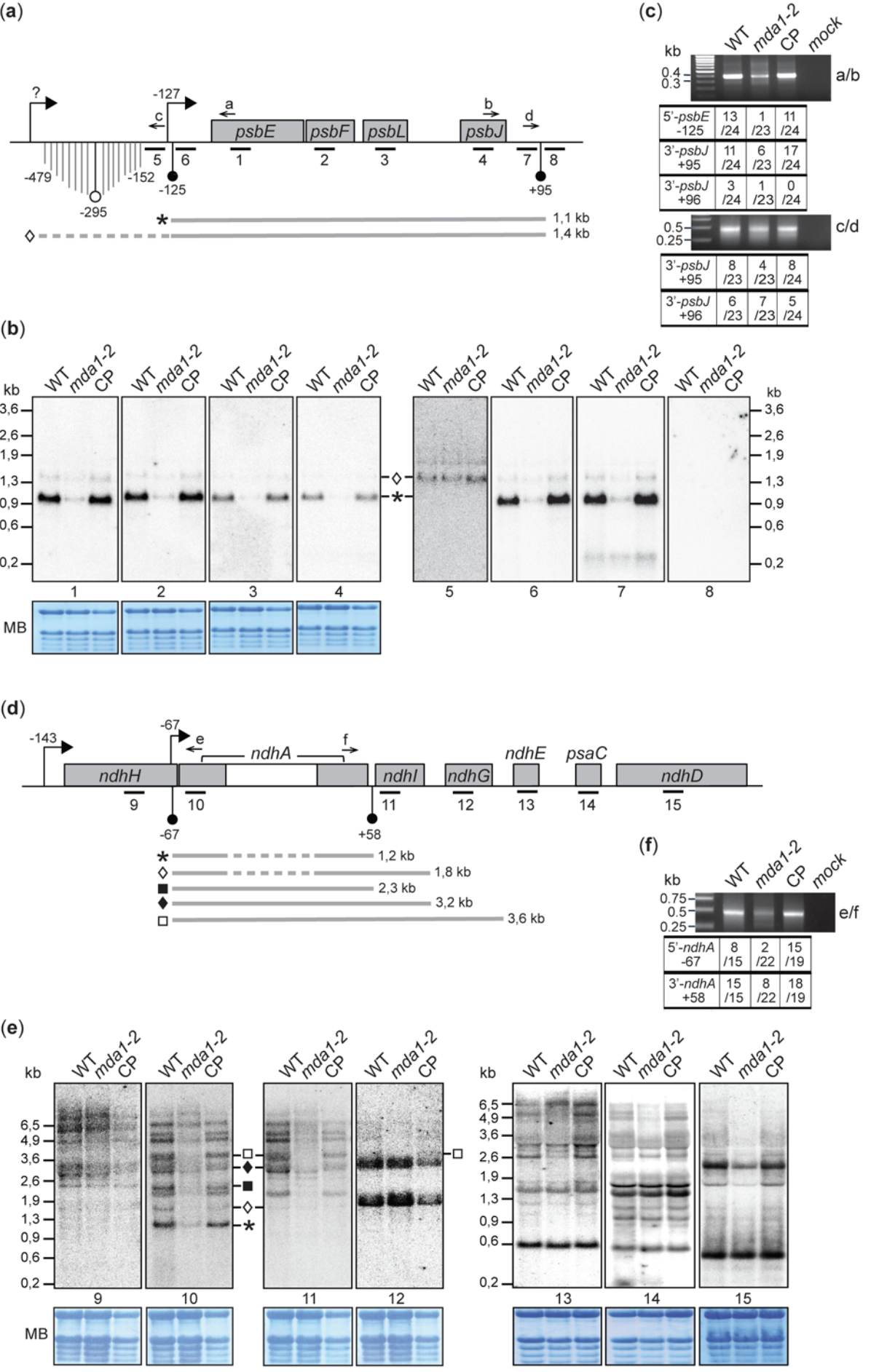
(a)
?
-127
c
a
b
d
psbE
psbF
psbL
psbJ
5
6
1
2
3
4
7
8
-479
-152
-295
-125
+95
1,1 kb
1,4 kb
(c)
kb
WT
mda1-2 CP
mock
0.4
0.3
a/b
5'-psbE -125 | 13 /24 | 1 /23 | 11 /24
3'-psbJ +95 | 11 /24 | 6 /23 | 17 /24
3'-psbJ +96 | 3 /24 | 1 /23 | 0 /24
0.5
0.25
c/d
3'-psbJ +95 | 8 /23 | 4 /23 | 8 /24
3'-psbJ +96 | 6 /23 | 7 /23 | 5 /24
(b)
kb
3,6
2,6
1,9
1,3
0,9
0,6
0,2
1
2
3
4
5
6
7
8
MB
(d)
-143
-67
e
f
ndhA
ndhH
ndhI
ndhG
ndhE
psaC
ndhD
9
10
11
12
13
14
15
-67
+58
1,2 kb
1,8 kb
2,3 kb
3,2 kb
3,6 kb
(f)
0.75
0.5
0.25
e/f
5'-ndhA -67 | 8 /15 | 2 /22 | 15 /19
3'-ndhA +58 | 15 /15 | 8 /22 | 18 /19
(e)
6,5
4,9
3,6
2,6
1,9
1,3
0,9
0,6
0,2

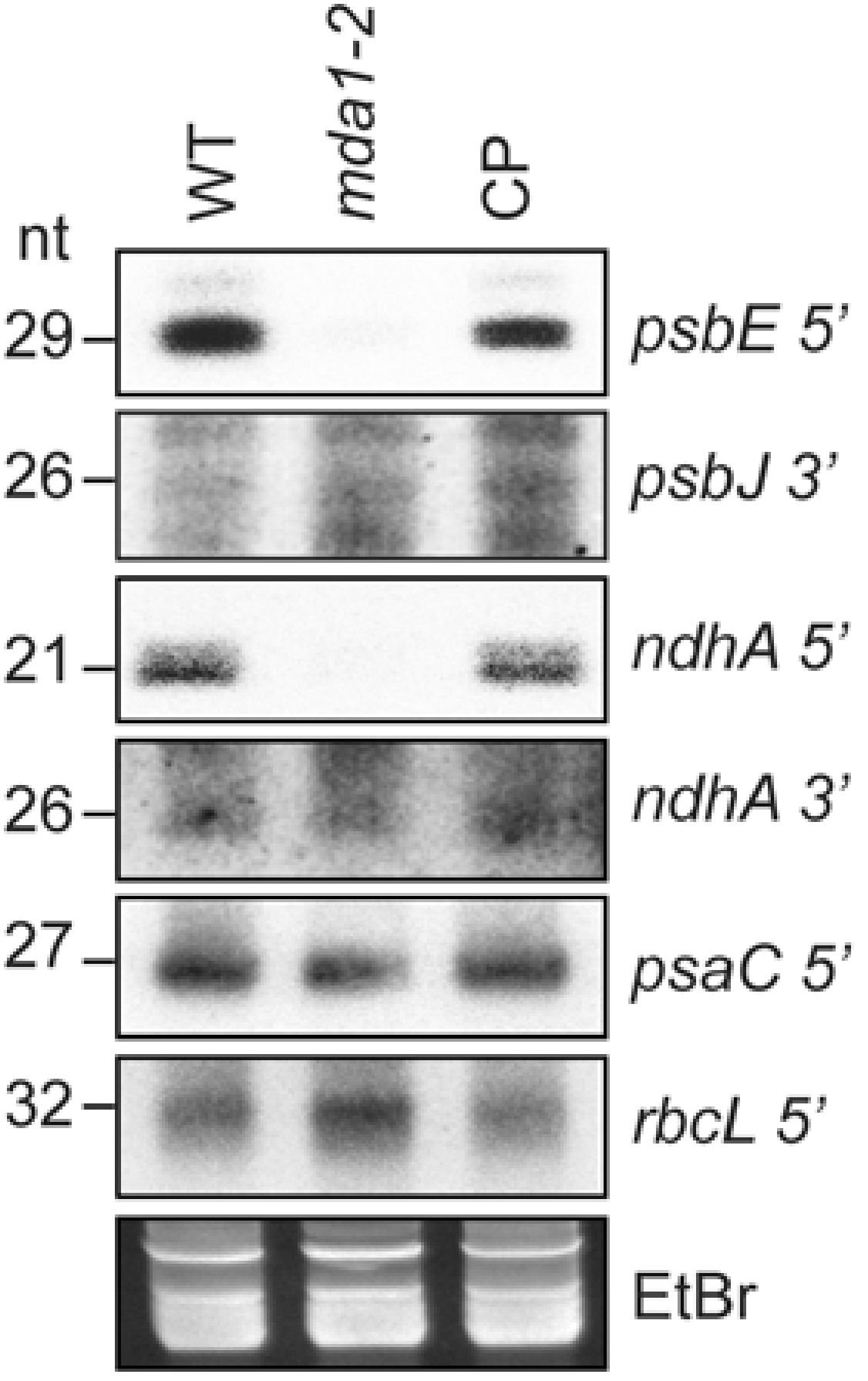
WT
mda1-2
CP
nt
29
psbE 5'
26
psbJ 3'
21
ndhA 5'
26
ndhA 3'
27
psaC 5'
32
rbcL 5'
EtBr

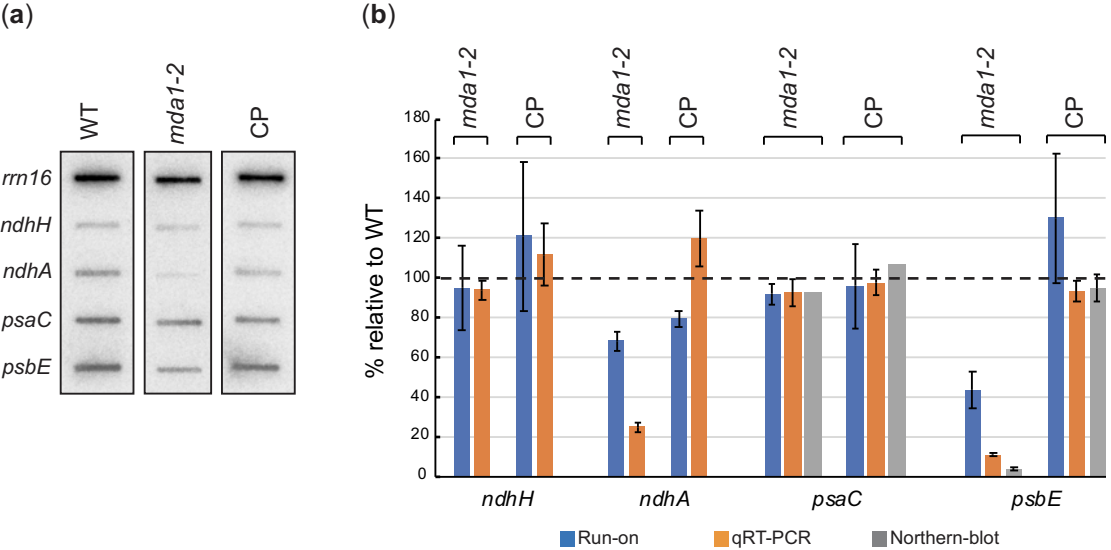
(a)
WT
mda1-2
CP
rrn16
ndhH
ndhA
psaC
psbE
(b)
mda1-2
CP
% relative to WT
180
160
140
120
100
80
60
40
20
0
ndhH
ndhA
psaC
psbE
Run-on
qRT-PCR
Northern-blot

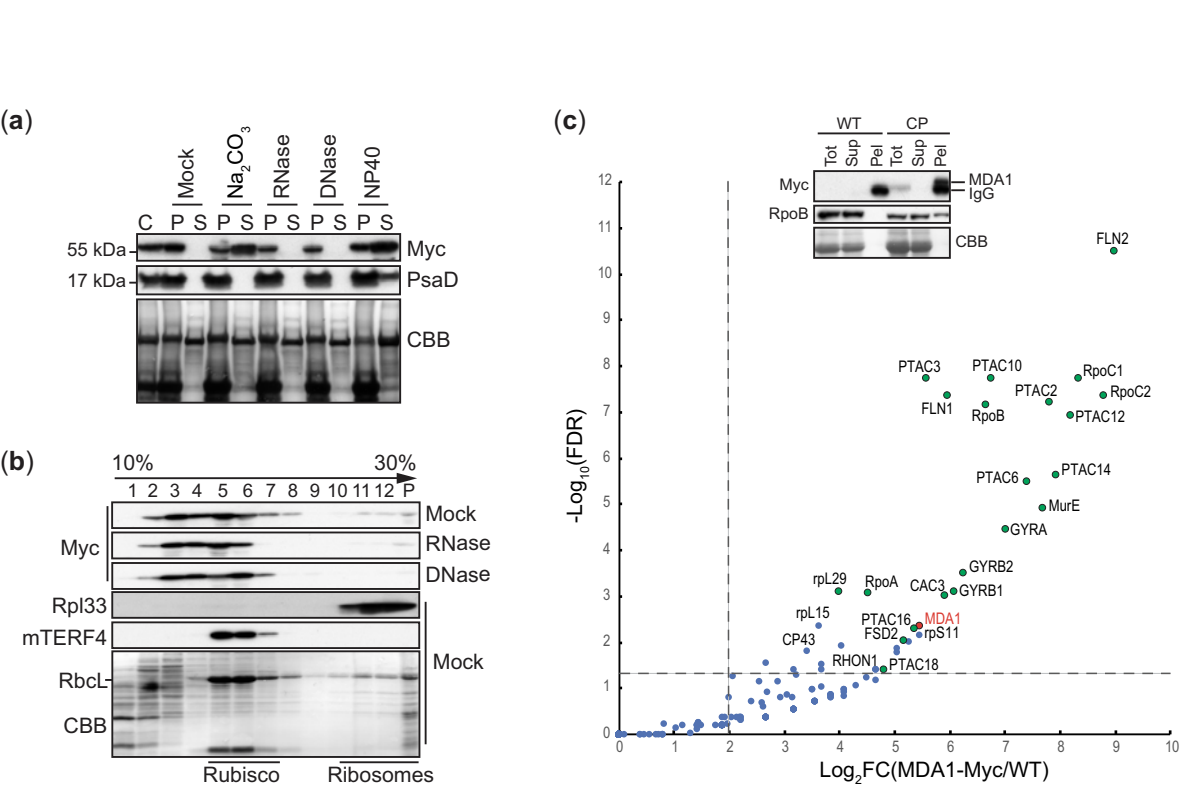
(a)
Mock
Na2CO3
RNase
DNase
NP40
C P S P S P S P S P S P S
55 kDa
17 kDa
Myc
PsaD
CBB
(b)
10%
30%
1 2 3 4 5 6 7 8 9 10 11 12 P
Mock
RNase
DNase
Myc
Rpl33
mTERF4
RbcL
CBB
Mock
Rubisco
Ribosomes
(c)
WT
CP
Tot Sup Pel Tot Sup Pel
Myc
RpoB
CBB
MDA1
IgG
-Log10(FDR)
Log2FC(MDA1-Myc/WT)
FLN2
PTAC3
PTAC10
RpoC1
PTAC2
RpoC2
FLN1
RpoB
PTAC12
PTAC6
PTAC14
MurE
GYRA
GYRB2
rpL29
RpoA
CAC3
GYRB1
rpL15
PTAC16
MDA1
FSD2
rpS11
CP43
RHON1
PTAC18

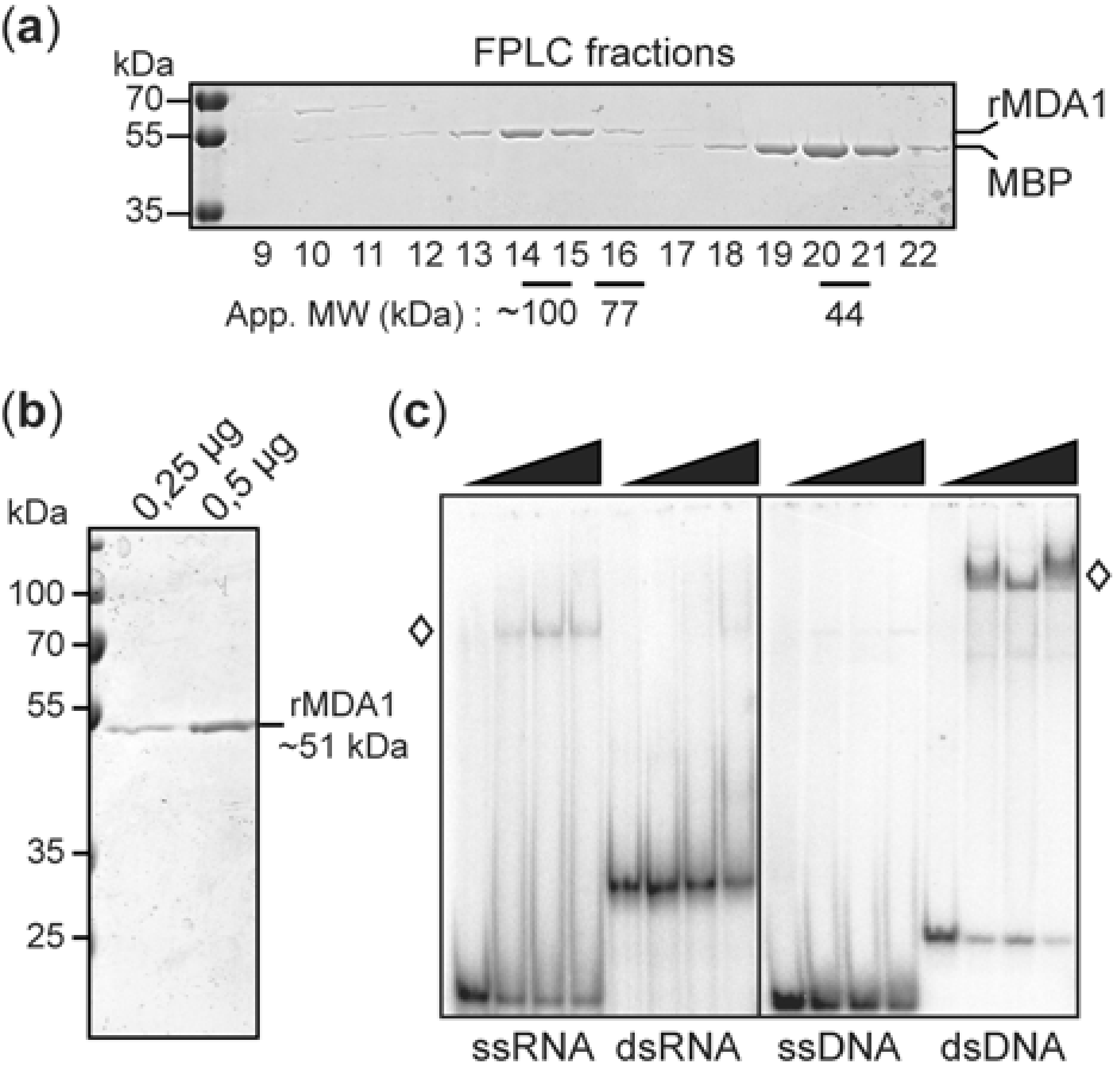
(a)
FPLC fractions
kDa
70
55
35
rMDA1
MBP
9 10 11 12 13 14 15 16 17 18 19 20 21 22
App. MW (kDa) : ~100 77 44
(b)
0,25 µg
0,5 µg
kDa
100
70
55
35
25
rMDA1
~51 kDa
(c)
ssRNA dsRNA ssDNA dsDNA

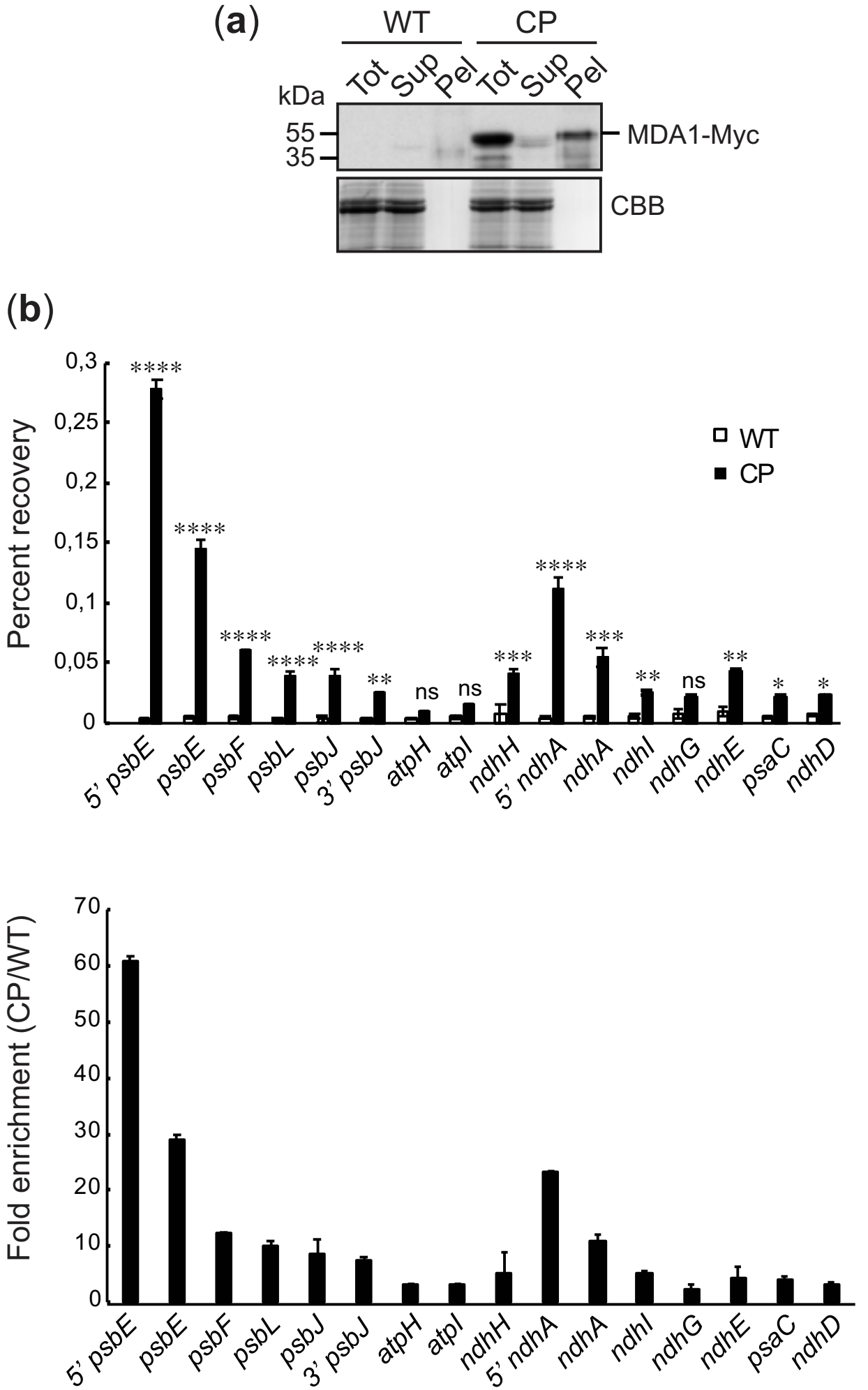
(a)
WT
CP
Tot
Sup
Pel
Tot
Sup
Pel
kDa
55
35
MDA1-Myc
CBB
(b)
Percent recovery
0,3
0,25
0,2
0,15
0,1
0,05
0
WT
CP
****
****
****
****
****
**
ns
ns
***
****
***
**
ns
**
*
*
5' psbE
psbE
psbF
psbL
psbJ
3' psbJ
atpH
atpI
ndhH
5' ndhA
ndhA
ndhI
ndhG
ndhE
psaC
ndhD
Fold enrichment (CP/WT)
70
60
50
40
30
20
10
0
5' psbE
psbE
psbF
psbL
psbJ
3' psbJ
atpH
atpI
ndhH
5' ndhA
ndhA
ndhI
ndhG
ndhE
psaC
ndhD

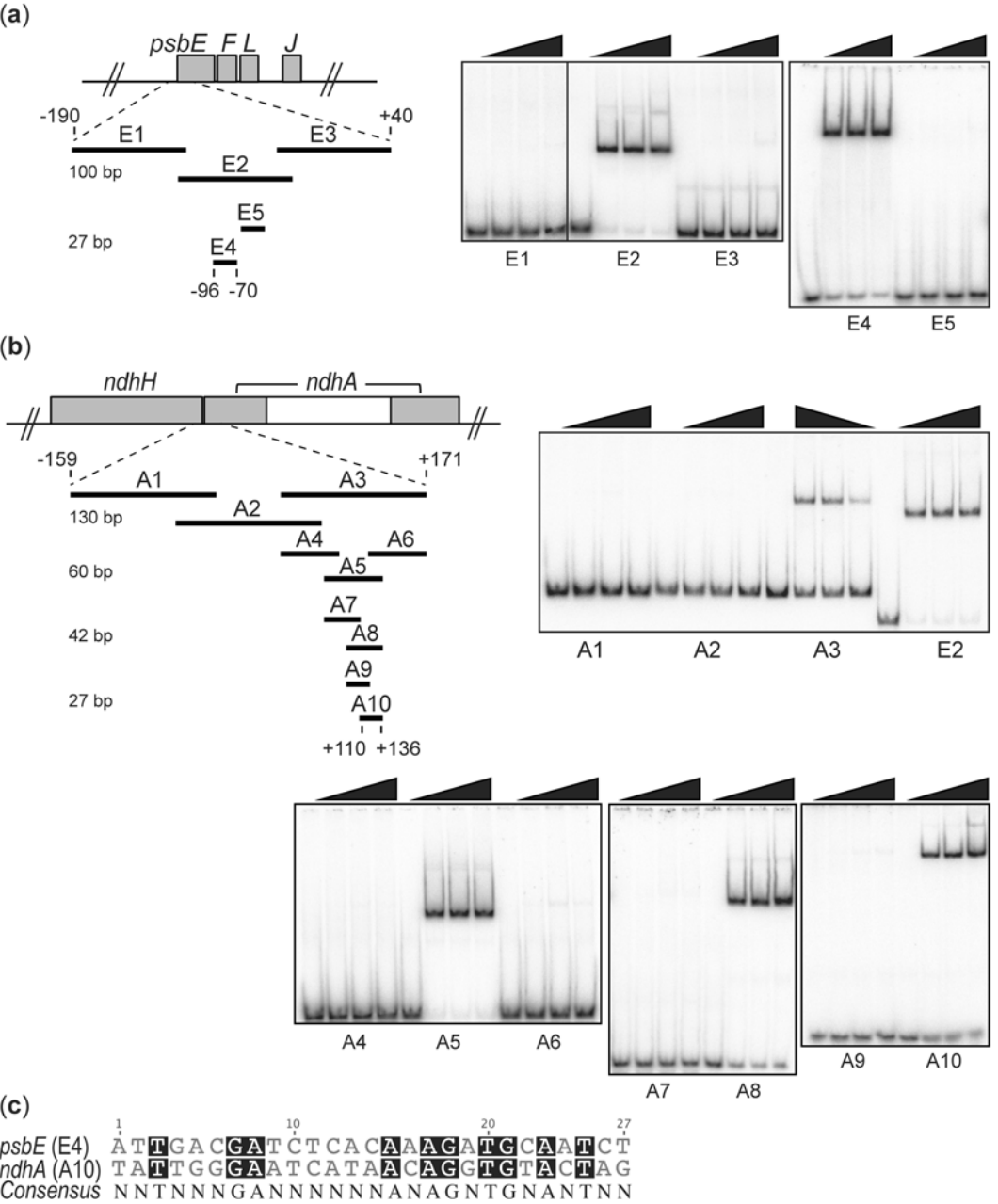
(a)
psbE F L J
-190
+40
E1
E3
E2
100 bp
E5
27 bp
E4
-96 -70
E1
E2
E3
E4
E5
(b)
ndhH
ndhA
-159
+171
A1
A3
A2
130 bp
A4
A6
60 bp
A5
A7
42 bp
A8
A9
27 bp
A10
+110 +136
A1
A2
A3
E2
A4
A5
A6
A7
A8
A9
A10
(c)
1
10
20
27
psbE (E4) ATTGACGATCTCACAAAGATGCAATCT
ndhA (A10) TATTGGGAATCATAACAGGTGTACTAG
Consensus NNTNNNGANNNNNNANAGNTGNANTNN

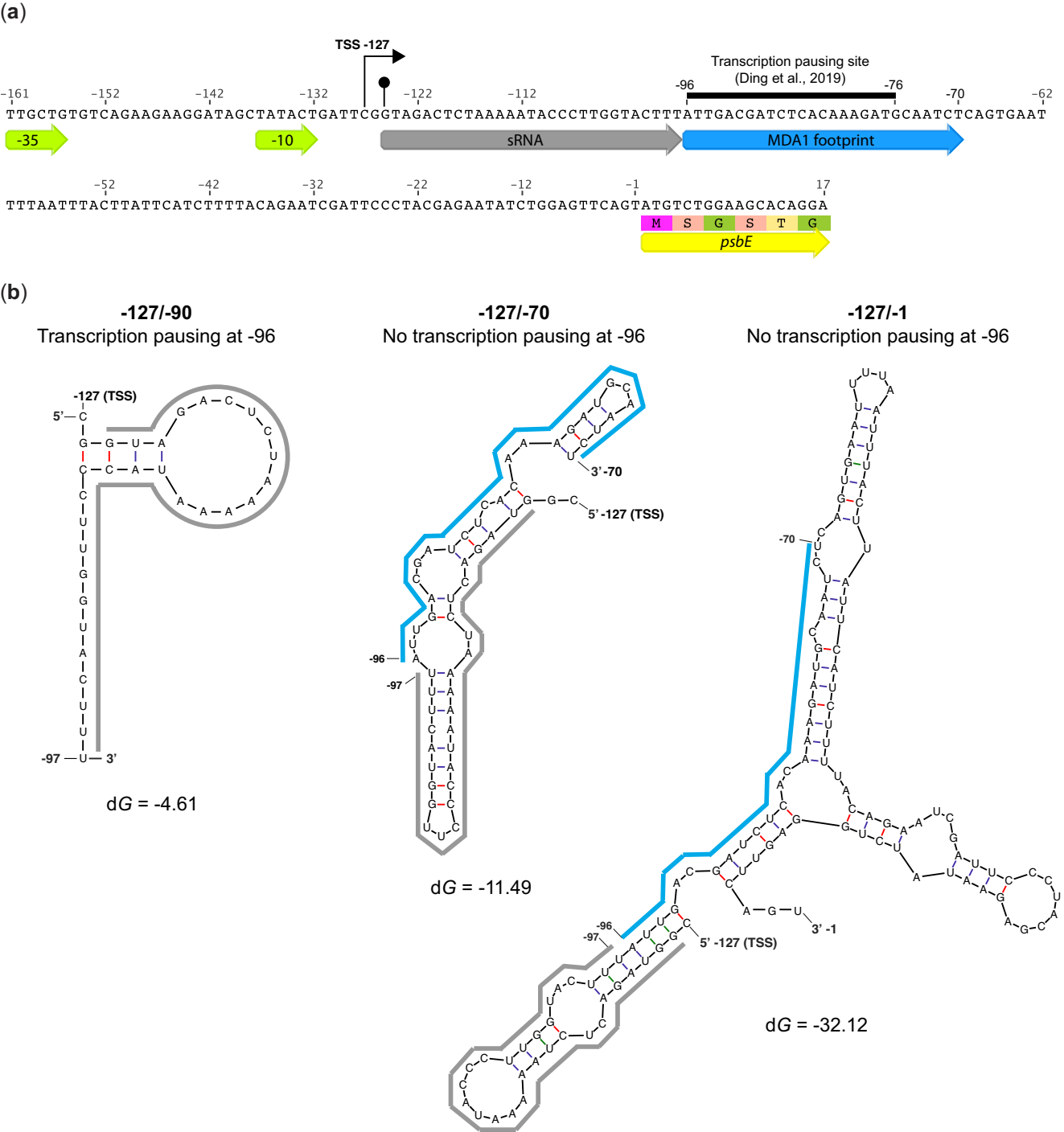
(a)
TSS -127
Transcription pausing site
(Ding et al., 2019)
-161
-152
-142
-132
-122
-112
-96
-76
-70
-62
TTGCTGTGTCAGAAGAAGGATAGCTATACTGATTCGGTAGACTCTAAAAATACCCTTGGTACTTTATTGACGATCTCACAAAGATGCAATCTCAGTGAAT
-35
-10
sRNA
MDA1 footprint
-52
-42
-32
-22
-12
-1
17
TTTAATTTACTTATTCATCTTTTACAGAATCGATTCCCTACGAGAATATCTGGAGTTCAGTATGTCTGGAAGCACAGGA
M
S
G
S
T
G
psbE
(b)
-127/-90
Transcription pausing at -96
-127 (TSS)
5'
-97
3'
dG = -4.61
-127/-70
No transcription pausing at -96
3' -70
5' -127 (TSS)
-96
-97
dG = -11.49
-127/-1
No transcription pausing at -96
-70
-96
-97
5' -127 (TSS)
3' -1
dG = -32.12